Biointerface Research in Applied Chemistry
Open-Access Journal (ISSN: 2069-5837)

Article
Volume 14, Issue 2, 2024, 47
https://doi.org/10.33263/BRIAC142.047

Exploring the Potential of Natural-like Compounds as TNF-α Inhibitors: An *In-silico* Approach

Vipul Agarwal[1], Mujeeba Rehman[1], Rishabh Chaudhary[1], Arjun Singh Kaushik[1], Mohd Usman Mohd Siddique[2], Siddhi Srivastava[1], Sukriti Srivastava[1], Vikas Mishra[1,*]

[1] Department of Pharmaceutical Sciences, Babasaheb Bhimrao Ambedkar University, Vidya Vihar, Raebareli Road, Lucknow-226025, (U.P.), India
[2] Department of Pharmaceutical Chemistry, Shri Vile Parle Kelavani Mandal's Institute of Pharmacy, Dhule Maharashtra, 424001, (U.P.), India
* Correspondence: vikasmishra12@gmail.com(V.M);

Scopus Author ID 56085576900
Received: 12.04.2023; Accepted: 24.06.2023; Published: 4.02.2024

Abstract: Tumor necrosis factor-α (TNF-α) regulates immune cells. Excessive production of TNF-α is associated with various diseases. TNF-α inhibition by antibodies or proteins directed against TNF-α is an accepted therapy for autoimmune diseases. However, the treatment above is expensive, with serious adverse effects. Moreover, no reported chemical inhibitors of TNF-α had been therapeutically successful. Thus, there is a need to explore cheap chemical compounds possessing anti-TNF-α activity with fewer side effects. This study aimed to identify novel natural-like compounds with TNF-α inhibitory activity using in-silico techniques. A library of 210 natural-like compounds was docked against TNF-α (PDB ID-2AZ5) using Glide. Based on the docking scores, the top 20 natural-like compounds with promising binding affinities (docking score <-6.5) were identified and subjected to ADMET profiling using SwissADME and pkCSM. The interactions of the compounds above were further validated by MM-GBSA and molecular dynamics using Prime-MMGBSA and Desmond (Schrödinger). ADMET profiling demonstrated that 7 natural-like compounds had excellent drug-like properties. The MM-GBSA and MD simulations finally revealed that 4 natural-like compounds, i.e., N-[(4Aminophenyl)methyl]adenosine, 5'-N Ethylcarboxamidoadenosine, Trifluridine, and APNEA, have strong protein-ligand interactions thus may act as potential TNF-α inhibitors. This study gives potential evidence for the effectiveness of these natural-like compounds as TNF-α inhibitors.

Keywords: docking; in-silico; ADMET screening; TNF-α; MM-GBSA; molecular dynamics

1. Introduction

Tumor necrosis factor alpha (TNF-α), also known as TNF superfamily member 2, is a highly potent and multifunctional proinflammatory cytokine. It plays a central biological role in the critical functioning of immune cells. Moreover, TNF-α is involved in various cellular activities, such as cell proliferation, metabolism, inflammation, differentiation, and apoptosis. TNF-α is a homotrimeric protein consisting of 157 amino acids that are predominantly produced by monocytic lineage cells, like macrophages, microglia, Kupffer cells, and many others, but can also be secreted in limited quantities by B cells, NK-cells, neutrophils, mast cells, endothelial cells,

cardiomyocytes, fibroblasts, osteoclasts, osteoblasts, astrocytes, dendritic cells, microglial cells, keratinocytes, and adipocytes [1–3]. It has been shown that cells do not store TNF-α; however, stimulation may initiate the de novo synthesis. The expression of TNF-α is controlled by various transcriptional, translational, and post-translational regulatory processes [4]. Upon activation through receptor binding, TNF-α has the potential to activate multiple immune signaling pathways. These include stimulation of c-Jun N-terminal kinase (JNK), nuclear factor kappa B (NFκB), mitogen-activated protein kinase (MAPK), and extracellular signal-regulated protein kinase (ERK) that are implicated in inflammation [5]. Dysregulation of TNF-α signaling is associated with multiple disease pathogenesis, such as inflammatory bowel disease, psoriasis, spondylitis, diabetes, asthma, systemic lupus erythematosus, chronic obstructive pulmonary disease (COPD), cancer, multiple sclerosis, and rheumatoid arthritis (RA) [6–9]. The levels of TNF-α are found to be significantly increased in patients suffering from diseases such as RA, breast cancer, and asthma [7,10–13]. Chronically stressed patients have also been reported to have higher TNF-α levels [14–19].

Over the past few years, many TNF-α blockers such as infliximab, etanercept, adalimumab, golimumab, and certonyzumab have revolutionized clinical interventions for various autoimmune disorders [20–22]. These drugs bind to the TNF-α dimer, which primarily inhibits the association of TNF-α with TNF-α receptors, thus downregulating the activation of downstream signaling complexes that trigger inflammation and other related pathways [23]. To date, the reported drugs are antibodies or proteins with high molecular weights, which are associated with numerous adverse effects, such as congestive heart failure, injection site reaction, and systematic side effects [24]. Moreover, most published small molecules explicitly target TNF-α via deregulation of its expression. Only a handful of compounds have been identified to inhibit this interaction, including polysulfonatednaphthylurea (suramin) and its analogues and indole-linked chromone (SPD304). However, the clinical uses of these small molecules are limited owing to low potency and poor selectivity, which tend to cause adverse effects such as bone marrow toxicity, nephrotoxicity with suramin, and cell toxicity with SPD304 [25].

Natural products (NPs) are an appealing source of active pharmaceutical ingredients because of their diverse structures, powerful biological activities, and favorable pharmacological profiles. However, the lengthy timeline and high expense of isolating and identifying naturally occurring substances have encouraged scientists to develop natural-like product libraries based on small molecules, taking stability enhancement and bioavailability into consideration. Moreover, two natural-like molecules (quinuclidine and indoloquinolizidine) [26], two FDA-approved compounds (ezetimibe and darifenacin), and iridium(III) biquinoline complex (metal-based) were described by Chan and his colleagues, which function as direct inhibitors of TNF-α [25,27,28].

Based on these findings, we conducted this cheminformatics study to explore several new natural-like compounds that may act as safe and novel TNF-α inhibitors.

2. Materials and Methods

2.1. Molecular docking studies.

2.1.1. Protein preparation.

The three-dimensional (3D) crystal structure of human TNF-α (PDB ID-2AZ5) [29–31] was retrieved from the protein data bank (https://www.rcsb.org/structure/2AZ5) [32]. The protein structure was then processed using Protein Preparation Wizard bundled with the Schrödinger Suite. First, the protein was pre-processed by assigning appropriate bond orders, incorporating hydrogen atoms, and generating disulfide bonds and zero-order bonds to metals. Water molecules larger than 5Å were removed from the het groups. Possible ionization states were generated in the protein structure using Epik, and the most stable state was selected [33]. Moreover, the Prime module of the Schrödinger Suite was utilized to fill in missing chains and loops. The chains with no active site residues were then trimmed. In the later stage, the sample water orientation was optimized, and protonation states were produced at pH 7.0 using PROPKA. Lastly, a controlled minimization was done using the OPLS3e force field to converge heavy atoms to a Root Mean Square Deviation (RMSD) value of 0.30Å [34–36].

2.1.2. Ligand preparation.

A library of 210 natural product-like compounds (Cat. No.: HY-L021L) was downloaded from MedChemExpress. The compounds were processed using the LigPrep Module of the Schrödinger Suite. The energy of the retrieved 3D structure was minimized and geometrically optimized, desalted, and further optimized for their proper chiralities and missing hydrogen atoms. The Epik package obtained possible ionization and tautomeric states between pH 6.8 and 7.2. Finally, the compounds were minimized to an RMSD of 1.8Å using the OPLS-2005 force field in the Schrödinger Suite to produce low-energy ligand isomers [37–40].

2.1.3. Active site prediction.

The processed protein structure was subjected to the SiteMap module in the Schrödinger Suite The top five active sites were identified. A minimum of 15 site points were expected for each reported site. Hydrophobicity and grid values were defined as more restricted and standard values, respectively. Moreover, site maps at 4Å from the closest site points were clipped. The best active site thus obtained was used for grid generation [41,42].

2.1.4. Receptor-ligand docking.

The processed ligands obtained through LigPrep were docked with TNF-α (PDB ID-2AZ5) using the Glide package of Schrödinger Suite [43,44]. The best-docked ligands were selected based on their docking scores. The docking score is based on receptor and ligand properties, including hydrogen bonds, extra precision (XP) penalties, electrostatic forces, lipophilic pockets, rotational penalties, etc. The XP mode and OPLS-3 power field were used to conduct the docking. The docking results were analyzed using the Glide module XP visualizer [35].

2.2. Absorption, distribution, metabolism, excretion, and toxicity (ADMET) profiling.

The ADMET characteristics of the selected ligands were determined using the free online web server SwissADME [45] from the Swiss Institute of Bioinformatics and pkCSM [46]. SwissADME forecasts physicochemical descriptors and predicts ADME parameters, pharmacokinetic properties, drug-like nature, and medicinal chemistry friendliness of one or more small molecules to support drug discovery. The SwissADME tool uses a vector machine (SVM) algorithm. Briefly, multiple molecules were entered into the SMILES list field according to their respective structures, followed by their submission to SwissADME calculations by clicking the run button. After completing the calculation within seconds, the output was compiled with all the values for each molecule, one molecule after the other. The data was then exported as a combined CSV file.

Moreover, the ADMET properties of the selected compounds were determined using the pkCSM web server. The pkCSM is a freely available machine-learning platform for analyzing and optimizing pharmacokinetics and toxicity properties using graph-based signatures. The SMILES string was provided to the web-server, and the prediction mode was selected as ADMET. The predictions containing all ADMET properties were displayed in tabular format immediately after the completion of the calculation [47–49].

2.3. Binding free energy.

The molecular mechanics-generalized born surface area (MM-GBSA) was used to measure the binding free energies of the protein-ligand complex using the Prime module of the Schrödinger Suite [50], which takes into account the VSGB dissolvable model and OPLS3 power field for analysis. The binding-free energy (ΔG_{bind}) of docked compounds was determined using equation (1) [51,52].

$$\Delta G_{bind} = \Delta E_{MM} + \Delta G_{solv} + \Delta G_{SA} \quad (1)$$

where ΔE_{MM}= difference in energy between the complex structure and the sum of the energies of the ligand and un-liganded protein using the OPLS force field.

ΔG_{solv}= difference in the GBSA solvation energy of the complex and the sum of the solvation energies for the ligand and un-liganded protein.

ΔG_{SA}= difference in the surface area energy for the complex and the sum of the surface area energies for the ligand and un-liganded protein.

2.4. Molecular dynamics (MD).

MD simulations were performed using the Desmond module of Schrödinger Suite A three-step procedure comprising a system builder, minimization, and molecular dynamics was used. Initially, the protein-ligand complex was prepared using a system builder. A single point charge (SPC) [53] was utilized as a solvent model in the system builder with an orthorhombic boundary box. Sodium and chloride ions were used to balance the charges. The model system was then subjected to energy minimization to eliminate steric clashes for a maximum of 2000 iterations. The simulation was performed under NPT ensemble for 50 ns.

Moreover, throughout the simulation, the Nose-Hoover thermostat algorithm and Martyna-Tobias-Klein barostat algorithm were used to maintain a constant temperature of 300 K and 1 atm of pressure, respectively. A cut-off value of 9.0 Å was used in the short-range method to assess the short-range coulombic interactions. The run was conducted for 50 ns, and 1000 frames were used to construct the trajectory [54–56]. After successful MD simulation, the file was processed using a Simulation Interaction Diagram (SID) to determine the stability of the simulated complex over the 50 ns simulations.

3. Results and Discussion

TNF-α is released in almost all inflammatory conditions and has a wide variety of biological activities that contribute to systemic symptoms (e.g., loss of appetite, fever, development of insulin resistance, metabolic abnormalities) and immunological changes (e.g., recruitment of neutrophils, increased phagocytosis, pro-inflammatory genes induction) [57]. FDA-approved TNF-α blockers, such as infliximab, adalimumab, and etanercept, are antibodies or proteins with a high molecular weight and a long list of side effects. Therefore, there is a need for novel molecules with anti-TNF-α activity and fewer adverse effects.

This study aimed to identify novel natural-like compounds with TNF-α inhibitory action using an *in-silico* approach. The 3D structure of the target protein TNF-α was downloaded from the RCSB protein data bank library and visualized (Figure 1A). The Ramachandran plot is a simple approach for visualizing the distribution of torsion angles in a protein structure. It also offers an overview of the permitted and prohibited areas of torsion angle values, which are crucial for determining the quality of three-dimensional protein structures [58]. In the Ramachandran plot of TNF-α, a residue of 90.2% was found in the most favored region, 9.6% in the additional allowed region, and 0.2% in the generously allowed region, indicating that it is a favorable protein for docking (Figure 1B) The raw protein was pre-processed using the Protein Preparation Wizard (Figure 1C). Chains C and D with no active site residue were trimmed (Figure 1D).

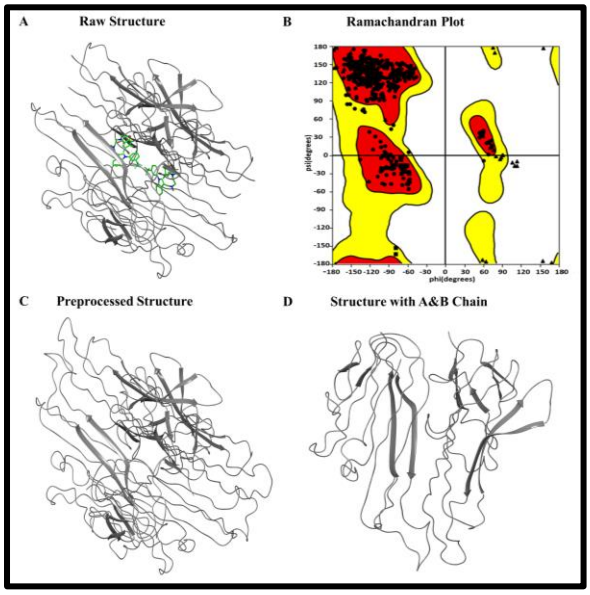

Figure 1. Structure of TNF-α (2AZ5). **(A)** Represents the raw structure of TNF-α with a small-molecule inhibitor retrieved from protein data bank **(B) (**Ramachandran plot for the predicted structure (**C)** represents the processed protein obtained following protein preparation wizard (**D)** represents the processed protein with A and B chain.

The active site was identified using the SiteMap module bundled with Schrödinger Suite. A total of 4 top potential druggable pockets on the surface were identified (Figure 2).

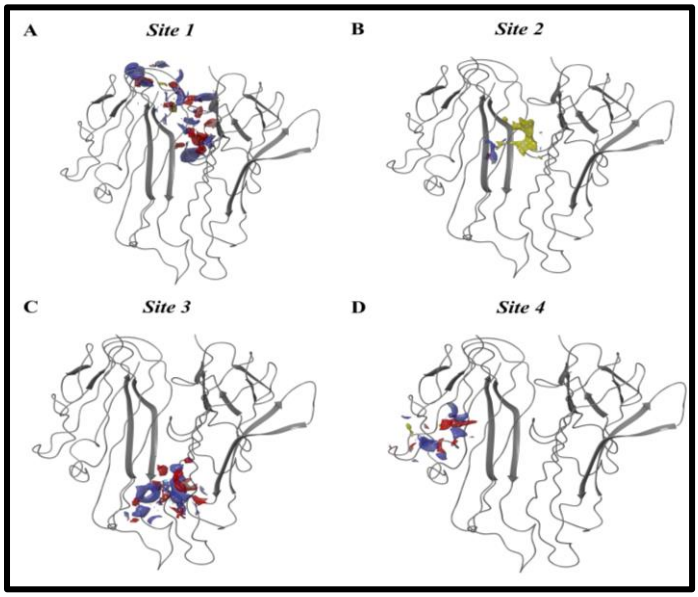

Figure 2. Active site detection using SiteMap. The figure shows 4 best active sites obtained by using the SiteMap module of Schrödinger.

Out of all, site 1 and site 2 had drug scores≈1 with a volume of 213.30 $Å^3$ and 173.59 $Å^3$, respectively (Table 1).

Table 1. Details of best 4 active sites of TNF-α using SiteMap.

Sites	Site Score	Size	D Sore	Volume(Å3)
Site 1	0.969	105	0.928	213.003
Site 2	0.858	38	0.909	173.558
Site 3	0.789	52	0.671	207.858
Site 4	0.585	26	0.541	80.948

Based on the literature, site 2 is preferred for designing inhibitors of TNF-α [29,59]. Hence, site 2 was used for grid generation using the Receptor Grid Generation Wizard of the Schrödinger Suite (Figure 3).

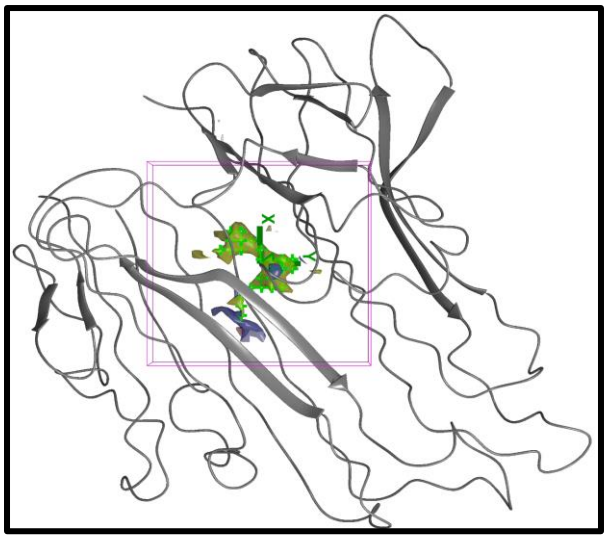

Figure 3. Grid Generation**.** The figure shows the grid used for docking.

A total of 210 natural-like compounds were included in this study. After successful docking, parameters such as docking score, ecoul (Coulomb energy), Glide evdw (Van Der Waals energy), Glide energy (Van Der Waals energy + Coulomb energy), and the interacting residues (hydrogen bonds) against TNF-α were determined. Binding affinities of the ligands with TNF-α were analyzed and evaluated based on their docking scores. Out of the 210 compounds, more than 50 compounds showed a docking score <-5; however, the top 20 compounds were selected for further investigation (Table 2).

The 2D structure, drawn using ChemDraw Ultra version 12 (CambridgeSoft) [60], and docking poses of all 20 compounds showing the best docking results with TNF-α are depicted in Figure 4 and Figure 5, respectively.

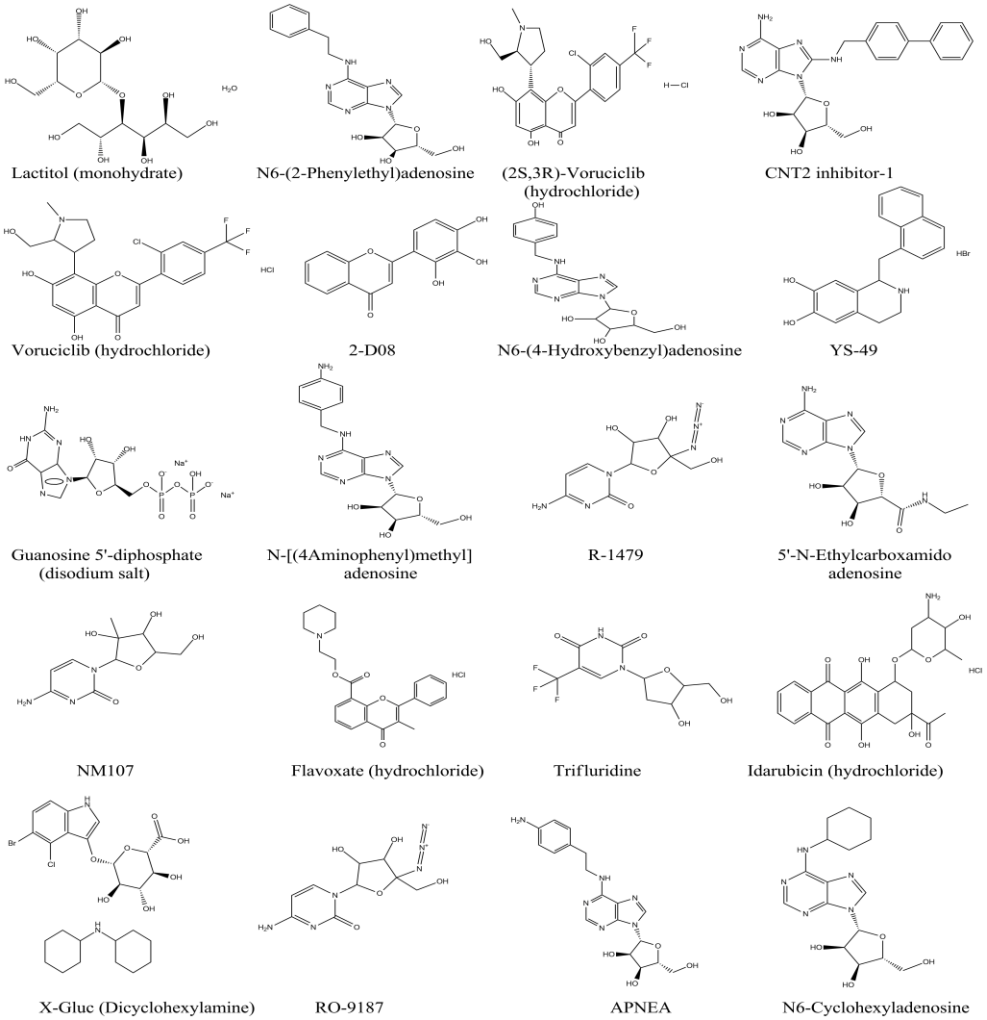

Figure 4. 2D structure of compounds. The figure shows the 2D structure of 20 compounds, showing the best docking result against TNF-α.

Table 2. Docking properties of selected compounds.

S. No.	Name	Glide Rotatable Bonds	Docking Score	Glide evdw	Glide ecoul	Glide Energy	Glide emodel	XP H Bond
1	Lactitol (monohydrate)	17	-8.68	-24.93	-12.314	-37.244	-44.714	-3.58
2	N6-(2-Phenylethyl)adenosine	9	-7.924	-32.221	-6.083	-38.304	-52.565	-0.96
3	(2S,3R)-Voruciclib (hydrochloride)	7	-7.917	-35.718	-6.178	-41.895	-56.206	-0.7
4	CNT2 inhibitor-1	9	-7.88	-35.636	-8.45	-44.085	-82.181	-1.19
5	Voruciclib (hydrochloride)	7	-7.879	-33.46	-8.692	-42.152	-50.072	-1.18

S. No.	Name	Glide Rotatable Bonds	Docking Score	Glide evdw	Glide ecoul	Glide Energy	Glide emodel	XP H Bond
6	2-D08	4	-7.376	-24.915	-10.983	-35.898	-44.059	-1.92
7	N6-(4-Hydroxybenzyl)adenosine	9	-7.116	-31.796	-7.212	-39.008	-53.335	-2.585
8	YS-49	4	-7.07	-25.723	-5.846	-31.569	-44.069	-0.96
9	Guanosine 5'-diphosphate (disodium salt)	9	-7.031	-28.488	-23.588	-52.076	-65.673	-3.11
10	N-[(4Aminophenyl)methyl]adenosine	8	-6.789	-32.256	-7.059	-39.315	-52.583	-2.045
11	R-1479	6	-6.762	-26.543	-10.059	-36.602	-42.144	-2.883
12	5'-N-Ethylcarboxamidoadenosine	6	-6.757	-32.509	-6.466	-38.976	-43.712	-1.189
13	NM107	5	-6.706	-24.311	-6.687	-30.998	-37.316	-2.4
14	Flavoxate (hydrochloride)	6	-6.697	-35.914	-1.617	-37.531	-52.618	0
15	Trifluridine	5	-6.673	-26.13	-4.587	-30.717	-38.418	-1.59
16	Idarubicin (hydrochloride)	7	-6.66	-35.317	-4.861	-40.177	-55.398	-0.96
17	X-Gluc (Dicyclohexylamine)	6	-6.608	-33.401	-5.38	-38.781	-50.398	-2.067
18	RO-9187	6	-6.603	-27.081	-8.93	-36.011	-46.357	-2.072
19	APNEA	9	-6.58	-33.117	-3.648	-36.764	-49.825	-1.646
20	N6-Cyclohexyladenosine	7	-6.542	-27.657	-5.579	-33.236	-43.591	-1.44

Docking score Docking score, including all additional terms; **Glide evdw** Van der Waals energy; **Glide ecoul** Coulomb energy; **Glide energy** Modified Coulomb-van der Waals interaction energy; **Glide emodel** Model energy, Emodel; **H Bond** H-bond pair term

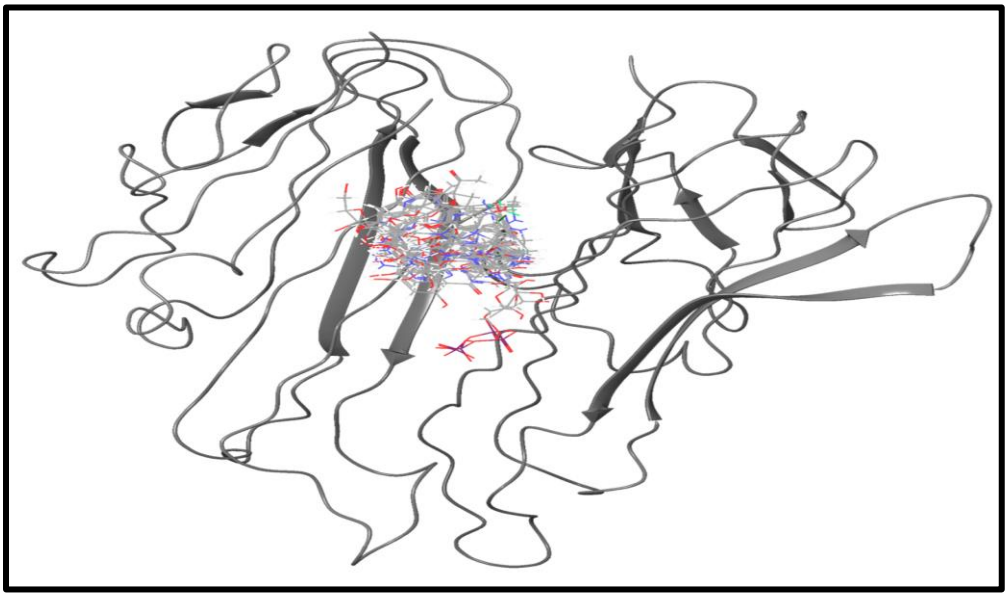

Figure 5. Dock poses of selected compounds**.** The figure represents 3D dock poses of the best 20 docked compounds against TNF-α.

All 20 compounds, including Lactitol (monohydrate), N6-(2-Phenylethyl)adenosine, (2S,3R)-Voruciclib (hydrochloride), CNT2 inhibitor-1, Voruciclib (hydrochloride), 2-D08, N6-(4-Hydroxybenzyl)adenosine, YS-49, Guanosine 5'-diphosphate (disodium salt), N-[(4Aminophenyl)methyl]adenosin R-1479, 5'-N-Ethylcarboxamidoadenosine, NM107, Flavoxate (hydrochloride), Trifluridine, Idarubicin (hydrochloride), X-Gluc (Dicyclohexylamine), RO-9187, APNEA and N6-Cyclohexyladenosine exhibited docking scores between -8.68 and -6.54. The good binding affinities were due to good hydrogen bonding, Coulomb energy, and Van der Waals forces (Table 2). The 3D docking poses and 2D interaction revealed that SER60, LEU59 TYR59, GLN61, TYR119, GLY121, and TYR151 in chain A and TYR59, LEU59, SER60, TYR119, and TYR151 in chain B play an important role in ligand binding (Figure 6-7, Table 3).

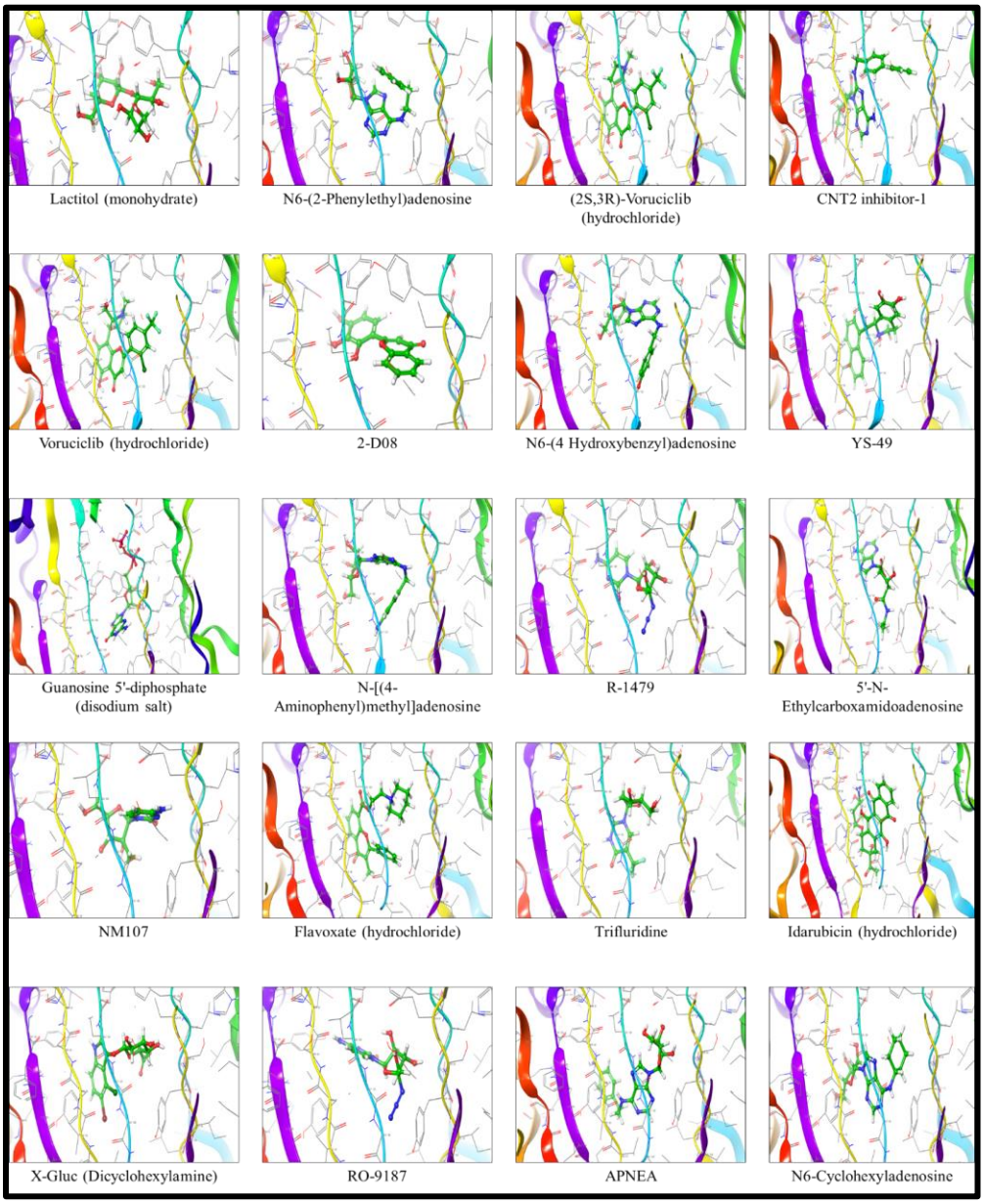

Figure 6. 3D docking poses of the top 20 docked compounds with TNF-α**.** The output of the Schrödinger 3D diagram showed the binding site residues of TNF-α with the top 20 docked compounds.

Table 3. List of top identified molecules with different types of interactions with active site residues (PDB 2AZ5).

S.No.	Name	No. of Contacts		Active Site Residues	
		HB	π- π	Chain A	Chain B
1	Lactitol (monohydrate)	4	-	TYR119, LEU120, GLY121, GLN61, SER60, TYR59,TYR151	TYR151, GLN61,SER60, TYR59, TYR119, LEU120, GLY121
2	N6-(2-Phenylethyl)adenosine	2	1	TYR119, LEU120, GLY121, GLN61, SER60, TYR59,TYR151	TYR151, GLN61,SER60, TYR59, TYR119, LEU120, GLY121
3	(2S,3R)-Voruciclib (hydrochloride)	1	1	TYR119, LEU120, LEU57, GLN61, SER60, TYR59,TYR151	TYR151, GLN61,SER60, TYR59, TYR119, LEU120, LEU57
4	CNT2 inhibitor-1	1	3	TYR119, LEU120, GLY121, GLN61, SER60, TYR59,TYR151	TYR151, GLN61,SER60, TYR59, TYR119, LEU120, GLY121

S.No.	Name	No. of Contacts		Active Site Residues	
		HB	π- π	Chain A	Chain B
5	Voruciclib (hydrochloride)	2	1	TYR119, LEU120, GLY121, GLN61, SER60, TYR59,TYR151	TYR151, GLN61,SER60, TYR59, TYR119, LEU120, GLY121
6	2-D08	2	2	TYR119, LEU120, GLY121, GLN61, SER60, TYR59,TYR151	TYR151, GLN61,SER60, TYR59, TYR119, LEU120, GLY121
7	N6-(4-Hydroxybenzyl)adenosine	2	-	TYR119, LEU120, GLY121, LEU57, SER60, TYR59,TYR151	TYR151, LEU57,SER60, TYR59, TYR119, LEU120, GLY121
8	YS-49	2	2	TYR119, LEU120, GLY121, LEU57, ILE155, TYR59,TYR151	TYR151, GLN61,SER60, TYR59, TYR119, LEU120, GLY121
9	Guanosine 5'-diphosphate (disodium salt)	3	-	TYR119, LYS98, GLY121	TYR151, GLN61,SER60, TYR59, TYR119, LEU120, GLY121, LYS98
10	N-[(4Aminophenyl)methyl] Adenosine	3	1	TYR119, LEU120, GLY121, GLN61, SER60, TYR59,TYR151	TYR151, GLN61,SER60, TYR59, TYR119, LEU120, GLY121
11	R-1479	3	-	TYR119, LEU120, GLY121, GLN61, SER60, TYR59,TYR151	TYR151, GLN61,SER60, TYR59, TYR119, LEU120, GLY121
12	5'-N-Ethylcarboxamidoadenosine	2	1	TYR119, LEU120, GLY121, GLN61, SER60, TYR59,TYR151	TYR151, GLN61,SER60, TYR59, TYR119, LEU120, GLY121
13	NM107	2	-	TYR119, LEU120, GLY121, GLN61, SER60, TYR59,TYR151	TYR151, GLN61,SER60, TYR59, TYR119, LEU120, GLY121
14	Flavoxate (hydrochloride)	-	3	TYR119, LEU120, GLY121, GLN61, SER60, TYR59,TYR151	TYR151, GLN61,SER60, TYR59, TYR119, LEU120, GLY121
15	Trifluridine	2	-	TYR119, LEU120, GLY121, GLY122, TYR59,LEU57	TYR151, GLN61,SER60, TYR59, TYR119, LEU120, GLY121
16	Idarubicin (hydrochloride)	1	-	TYR119, LEU120, GLY121, GLN61, SER60, TYR59, TYR151	TYR151, GLN61,SER60, TYR59, TYR119, LEU120, GLY121
17	X-Gluc (Dicyclohexylamine)	4	1	TYR119, LEU120, GLY121, GLN61, SER60, TYR59, TYR151, LEU 59	TYR151, GLN61,SER60, TYR59, TYR119, LEU120, GLY121, LEU59
18	RO-9187	4	-	TYR119, LEU120, GLY121, GLN61, SER60, TYR59, TYR151	TYR151, GLN61,SER60, TYR59, TYR119, LEU120, GLY121
19	APNEA	-	1	TYR119, LEU120, GLY121, TYR59,LEU57, TYR151	TYR151, GLN61,SER60, TYR59, TYR119, LEU120, GLY121
20	N6-Cyclohexyladenosine	2	-	TYR119, LEU120, GLY121, GLN61, SER60, TYR59, TYR151	TYR151, GLN61,SER60, TYR59, TYR119, LEU120, GLY121

HB No. of hydrogen bond

π- π No. of pi-pi stacking

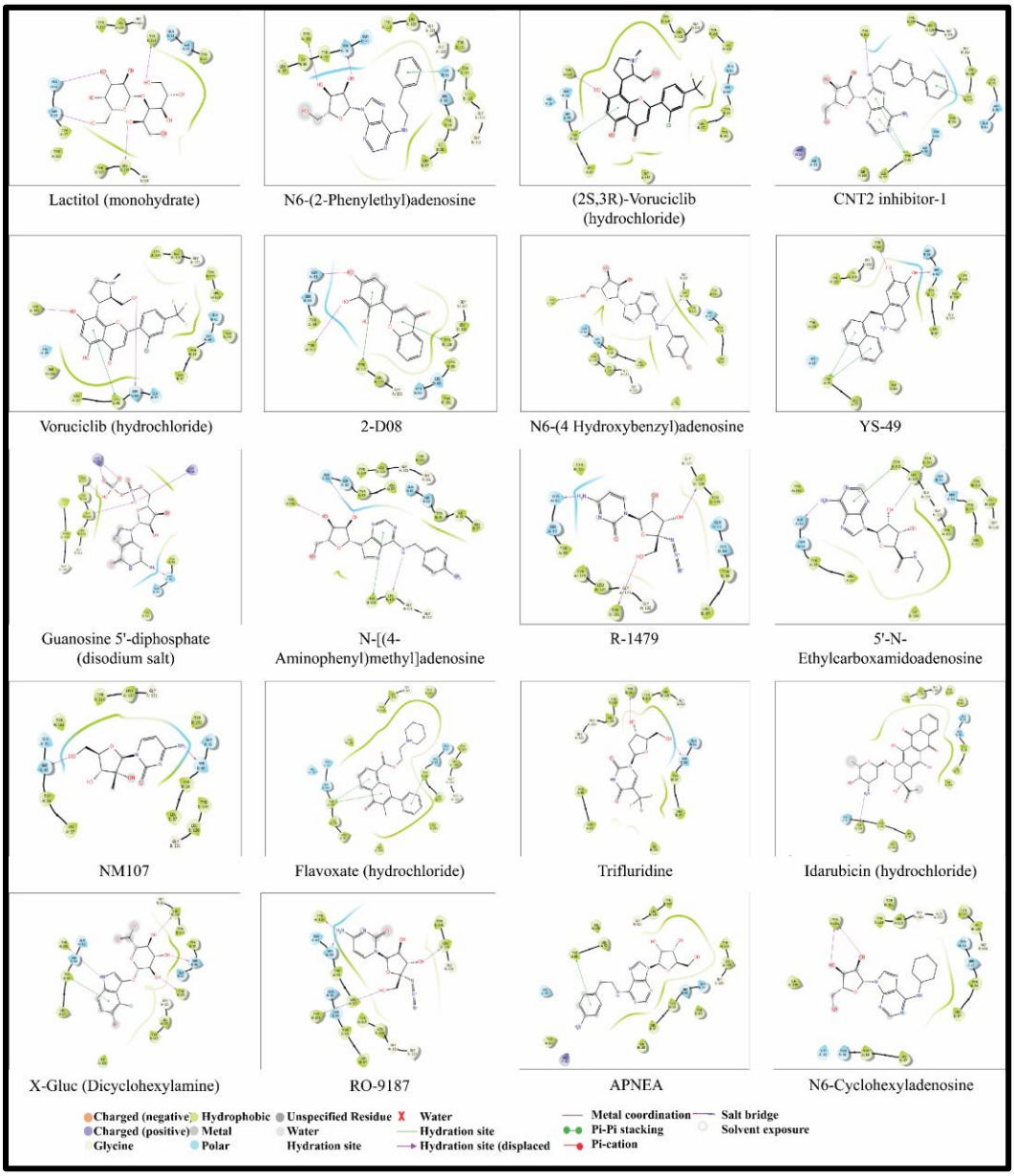

Figure 7. 2D interaction of top 20 docked compounds with TNF-α**.** The output of Schrödinger 2D interaction diagram of TNF-α with the top docked compounds.

The Lactitol monohydrate is a disaccharide analog of lactulose. It is used to treat hepatic encephalopathy and constipation. The docking score for Lactitol monohydrate was found to be -8.68. The docking score was attributed to 4 hydrogen bond formations between Lactitol monohydrate and TNF-α at Tyrosine and Leucine at chain A with Serine and Guanidine at Chain B (Figure 6-7). N6-(2-Phenylethyl)adenosine is an adenosine receptor (AR) agonist having Ki values of 11.8 nM, 30.1 nM, 0.63 nM for rat A1AR (A1 adenosine receptors), human A1AR and hA3AR (human A3 adenosine receptor), respectively. The docking score for N6-(2-Phenylethyl)adenosine was observed to be -7.92. The docking score was attributed to 2 hydrogen bonds at Serine and Tyrosine, along with good Van der Waals energy (Figure 6-7, Table 2-3). (2S,3R)-Voruciclib hydrochloride is the enantiomer of Voruciclib hydrochloride. (2S,3R)-Voruciclib is an orally active cyclin-dependent kinase (CDK) inhibitor that ultimately blocks cell

cycle and inhibits cell proliferation. The docking score for (2S,3R)-Voruciclib hydrochloride was -7.92. The docking score was attributed to 1 hydrogen bond formation between (2S,3R)-Voruciclib hydrochloride and TNF-α at Tyrosine at chain A along with good Van der Waals energy (Figure 6-7, Table 2-3). CNT2 inhibitor-1 is a potent concentrative nucleoside transporter 2 Inhibitor (CNT2). CNT2 inhibitor-1 exhibits inhibitory activity 1500-fold more potent than 2'-deoxy-5-fluorouridine, phlorizin, and 7,8,3'-trihydroxyflavone, well-known human CNT2 inhibitors. The docking score for CNT2 inhibitor-1 was observed to be -7.88. The docking score was attributed to 1 hydrogen bond between CNT2 inhibitor-1 and TNF-α at Tyrosine at chain A along with 3 pi-pi stacking (Figure 6-7, Table 2-3). 2-D08 is a cell-permeable, mechanistically unique inhibitor of protein SUMOylation. 2-D08 inhibits sumoylation by preventing the transfer of SUMO from the UBC9-SUMO thioester to the substrate. The docking score for 2-D08 was observed to be -7.34. The docking score was attributed to 2 hydrogen bonds and 2 pi-pi stacking (Figure 6-7, Table 2-3). N-[(4-Aminophenyl)methyl]adenosine is an adenosine receptor inhibitor. The docking score for N-[(4-Aminophenyl)methyl]adenosine was -6.79. The docking score was attributed to 3 hydrogen bonds and 1 pi-pi stacking (Figure 6-7, Table 2).

The success of a drug candidate is driven not only by its high potential but also by its favorable ADMET profile. A variety of ADME tools are accessible, which can predict several crucial aspects in silico and help analyze important characteristics of molecules. Nowadays, computational ADME is advised to be used early in the drug development process and should be performed in conjunction with in vivo and in vitro studies to limit the number of safety problems [61,62]. In the current study, ADMET profiling was performed using freely accessible online web servers, viz. SwissADME and pkCSM. According to the pharmacokinetic analysis, all compounds had noblood–brain barrier (BBB) permeability except YS-49 and Flavoxate (hydrochloride). Moreover, most compounds showed no inhibition of cytochrome P450 isomers (CYP2C9). CYP2C9 is a major cytochrome P450 enzyme involved in the metabolic clearance of a wide variety of therapeutic agents, including NSAIDS, oral anticoagulants, and oral hypoglycemics. Inhibition of CYP2C9 activity results in decreased metabolism of therapeutic agents, thus enhancing their plasma concentration, which may cause serious adverse effects. Thus, not having CYP2C9 inhibitory action by natural-like compounds suggests low chances of drug interactions utilizing the CYP2C9 enzymatic pathway for metabolism [63–65] (Table 4).

Table 4. ADMET properties of selected compounds using SwissADME.

S.No.	Name	Mol. Weight	No. of Heavy atoms	Molar Refractivity	CYP 2C9 inhibitor	BBB permeability	Log S (ESOL)	Sol. Class	No. of Lipinski Violations	Synthetic Accessibility	Bioavailability Score
1	Lactitol (monohydrate)	362.33	24	73.36	No	No	2.02	HS	2	5.48	0.17
2	N6-(2-Phenylethyl)adenosine	371.39	27	96.87	No	No	-3.15	S	0	4.29	0.55
3	(2S,3R)-Voruciclib (hydrochloride)	506.3	33	123.8	No	No	-6.19	PS	1	4.52	0.55
4	CNT2 inhibitor-1	448.47	33	121.9	No	No	-4.2	MS	0	4.75	0.55

S.No.	Name	Mol. Weight	No. of Heavy atoms	Molar Refractivity	CYP 2C9 inhibitor	BBB permeability	Log S (ESOL)	Sol. Class	No. of Lipinski Violations	Synthetic Accessibility	Bioavailability Score
5	Voruciclib (hydrochloride)	506.3	33	123.8	No	No	-6.19	PS	1	4.52	0.55
6	2-D08	270.24	20	73.99	No	No	-3.61	S	0	2.94	0.55
7	N6-(4-Hydroxybenzyl)adenosine	373.36	27	94.09	No	No	-2.71	S	0	4.17	0.55
8	YS-49	386.28	24	106.67	No	Yes	-5.64	MS	0	2.92	0.55
9	Guanosine 5'-diphosphate (disodium salt)	487.16	30	84.26	No	No	0.23	HS	1	4.57	0.11
10	N-[(4Aminophenyl)methyl]adenosine	372.38	27	96.47	No	No	-2.5	S	0	4.24	0.55
11	R-1479	284.23	20	60.71	No	No	-0.47	VS	1	4.17	0.11
12	5'-N-Ethylcarboxamidoadenosine	308.29	22	74.13	No	No	-1.36	VS	0	4	0.55
13	NM107	257.24	18	60.69	No	No	-0.01	VS	0	3.99	0.55
14	Flavoxate (hydrochloride)	427.92	30	124.67	No	Yes	-5.7	MS	0	3.8	0.55
15	Trifluridine	296.2	20	58.11	No	No	-1.41	VS	0	3.71	0.55
16	Idarubicin (hydrochloride)	533.95	37	131.97	No	No	-4.87	MS	1	5.71	0.55
17	X-Gluc (Dicyclohexylamine)	603.93	37	144.14	No	No	-5.07	MS	2	5.51	0.17
18	RO-9187	284.23	20	60.71	No	No	-0.47	VS	1	4.17	0.11
19	APNEA	386.41	28	101.27	No	No	-2.8	S	0	4.35	0.55
20	N6-Cyclohexyladenosine	349.38	25	89.5	No	No	-2.91	S	0	4.42	0.55

HS Highly Soluble; **VS** Very Soluble; **S** Soluble; **MS** Moderately Soluble; **PS** Partially Soluble

Molar refractivity measures the overall polarity of a molecule and should be between 40 and 130. In the present study, most of the selected compounds' molar refractivity was within the acceptable range except for Idarubicin (hydrochloride) and X-Gluc (Dicyclohexylamine). The aqueous solubility of a compound significantly affects its absorption and distribution characteristics. The water solubility (logS) of a compound represents the solubility of the molecules in water at 25°C. Lipid-soluble drugs are absorbed less effectively than water-soluble drugs, particularly when administered orally. For solubility, log S, calculated using the ESOL model, should not exceed 6. Lactitol (monohydrate) and Guanosine 5'-diphosphate (disodium salt) showed Log S of 2.02 and 0.24, respectively, belonging to the highly soluble class. Compounds R-1479, 5'-N-Ethylcarboxamidoadenosine, NM107, Trifluridine, and RO-9187 belong to the very soluble class. The compounds APNEA, N6-(2-Phenylethyl)adenosine, N-[(4Aminophenyl)methyl]adenosine, N6-(4-Hydroxybenzyl)adenosine, and 2-D08 showed Log S (ESOL) values in the range of -2 to -4; hence all these compounds were found to be soluble. Drug-likeness prediction was further conducted using Lipinski's Rule and bioavailability score. Lipinski's Rule of Five indicates that a molecule's absorption is more probable when its molecular

weight is less than 500 g/mol, has a log P-value less than 5, and the molecule contains no more than 5 H-donor and 10 H-acceptor atoms. Most of the compounds had no Lipinski violations except Lactitol (monohydrate), (2S,3R)-Voruciclib (hydrochloride), Voruciclib (hydrochloride), Guanosine 5'-diphosphate (disodium salt), R-1479, Idarubicin (hydrochloride), X-Gluc (Dicyclohexylamine) and RO-9187. Bioavailability score predicts the probability of a compound having at least 10% oral bioavailability in rats or measurable Caco-2 cell (human colon adenocarcinoma) permeability. The bioavailability score of most of the selected compounds was 0.55, indicating the presence of drug-like properties (Table 4). Synthetic accessibility (SA) is essential in drug design, as computer-designed compounds cannot be synthesized in certain cases. The SA scores vary from 1 (extremely easy) to 10 (extremely difficult). All 20 selected compounds exhibited SA scores between 2.92 and 5.71, indicating ease of synthesis with all the selected compounds (Table 3). The primary site for the absorption of drugs for an orally delivered solution is the intestine. The percentage of chemicals absorbed by the human small intestine was predicted using pkCSM. Our results showed that most of the selected natural-like compounds had an intestinal absorption of >30% (Table 5).

Table 5. ADMET properties of selected compounds using pkCSM.

S. No.	Name	Mol. Weight	No. of Rot. Bond	Intestinal Absorption (Human)	Skin Permeability	*hERG I* inhibitor	AMES toxicity	Renal OCT2 substrate	Oral Rat Acute Toxicity (LD50)	Oral Rat Chronic Toxicity (LOAEL)	Skin Sensation
1	Lactitol (monohydrate)	362.328	8	13.262	-2.735	No	No	No	1.857	4.274	No
2	N6-(2-Phenylethyl) adenosine	371.397	6	69.457	-2.735	No	No	No	2.119	1.887	No
3	(2S,3R)-Voruciclib (hydrochloride)	506.304	3	84.469	-2.735	No	No	No	2.892	2.337	No
4	CNT2 inhibitor-1	448.483	6	70.688	-2.735	No	Yes	No	2.457	2.705	No
5	Voruciclib (hydrochloride)	506.304	3	91.421	-2.74	No	No	No	2.756	0.785	No
6	2-D08	270.24	1	95.878	-2.736	No	No	No	2.33	2.464	No
7	N6-(4-Hydroxybenzyl)adenosine	373.369	5	57.571	-2.735	No	Yes	No	2.473	3.741	No
8	YS-49	386.289	2	90.284	-2.751	Yes	Yes	No	2.552	1.029	No
9	Guanosine 5'-diphosphate (disodium salt)	487.166	6	0	-2.735	No	No	No	2.099	3.359	No
10	N-[(4Aminophenyl)methyl]adenosine	372.385	5	60.728	-2.735	No	No	No	2.329	1.748	No
11	R-1479	284.232	3	56.73	-2.736	No	No	No	1.748	2.459	No
12	5'-N-Ethylcarboxamidoadenosine	308.298	3	59.017	-2.735	No	No	No	2.032	1.517	No
13	NM107	257.246	2	53.622	-2.739	No	No	No	2.277	2.736	No
14	Flavoxate (hydrochloride)	427.928	5	96.049	-2.561	No	No	Yes	2.636	0.998	No

S. No.	Name	Mol. Weight	No. of Rot. Bond	Intestinal Absorption (Human)	Skin Permeability	*hERG I* inhibitor	AMES toxicity	Renal OCT2 substrate	Oral Rat Acute Toxicity (LD50)	Oral Rat Chronic Toxicity (LOAEL)	Skin Sensation
15	Trifluridine	296.201	2	62.768	-2.873	No	No	No	2.498	2.764	No
16	Idarubicin (hydrochloride)	533.961	3	70.711	-2.735	No	No	No	2.37	2.999	No
17	X-Gluc (Dicyclohexylamine)	603.938	5	21.561	-2.735	No	No	No	2.066	2.156	No
18	RO-9187	284.232	3	56.73	-2.736	No	No	No	1.748	2.459	No
19	APNEA	386.412	6	54.003	-2.735	No	No	No	2.343	1.695	No
20	N6-Cyclohexyladenosine	349.391	4	72.651	-2.735	No	Yes	No	2.109	2.163	No

Skin permeability is an essential factor for the effectiveness of many drugs and is relevant for developing transdermal drug delivery systems. pkCSM estimates the skin permeability constant logKp (cm/h) to determine whether a particular substance will likely be skin permeable. A substance with a logKp >-2.5 is regarded to have comparatively poor skin permeability. pkCSM analysis revealed that all 20 natural-like compounds had logKp <-2.5, indicating effective skin permeation ability (Table 4). The development of severe long QT syndrome, which leads to lethal ventricular arrhythmia, is mainly caused by inhibiting potassium channels encoded by hERG (human ether-a-go-go-related gene). Many drugs have been withdrawn from the pharmaceutical market because of their hERG channel inhibitory properties [66,67]. None of the selected natural-like compounds in our study had hERG inhibitory properties except YS-49 (Table 5). The Ames test is a biological experiment to determine the mutagenic potential of chemicals utilizing bacteria (Salmonella typhimurium). This test is necessary before clinical investigations, and a negative result is required for most regulatory bodies, including the US Food and Drug Administration (FDA). A negative Ames test was observed for most of the selected natural-like compounds except YS-49, N6-(4-Hydroxybenzyl)adenosine, CNT2 inhibitor-1, and N6-Cyclohexyladenosine. Organic Cation Transporter 2 (OCT-2) is a renal uptake transporter involved in the disposition and renal clearance of pharmaceuticals and endogenous chemicals [68]. OCT-2 substrates have the potential to interact negatively with OCT-2 inhibitors when taken together. Assessing a drug candidate's ability to be carried out by OCT-2 provides valuable information about the clearance as well as any possible contraindications of that drug. ADMET analysis showed that most of the selected compounds did not have the potential to act as OCT-2 substrates, indicating fewer chances of contradictions. Moreover, it is critical to examine the toxic potential of compounds. The lethal dose value (LD50) is a typical method used for determining the acute toxicity of a compound. The LD50 value is the dose of a chemical that kills 50% of set of test animals when administered all at once. The LD50 of the selected compounds was found in the range between 1.8 mol/kg and 2.9 mol/kg. In many therapeutic techniques, long-term exposure to low to moderate doses of chemicals is a serious problem. Therefore, chronic toxicity studies are designed to determine the lowest dose of a substance that may cause an adverse effect (lowest-observed-adverse-effect level viz. LOAEL). The chronic toxicity study of the selected compounds in log (mg/kg bw/day) was found

in the range of 0.8 mol/kg to 3.7 mol/kg, indicating a good safety profile of most of the compounds (Table 4). In addition, dermally applied products may also cause skin sensitization. Thus, one of the major safety concerns is to determine wheather a substance that comes into contact with the skin might cause allergic reactions. ADMET profiling revealed that none of the selected natural-like compounds had the potential to cause skin sensitivity. Complete ADMET profiling, as revealed by SwissADME and pKCSM suggested that 7 compounds, i.e., N6-(2-Phenylethyl)adenosine, 2-D08, N-[(4Aminophenyl)methyl]adenosine, 5'-N-Ethylcarboxamidoadenosine, NM107, Trifluridine, and APNEA have excellent drug-like properties and hence were used for further investigation. MM/GBSA calculations were used to determine the relative binding affinities of ligands to the target receptor. Theoretically, MM/GBSA can be used to rank ligands belonging to a congeneric series based on their free energy [69]. The binding energy estimations are improved by MM-GBSA analysis over molecule docking energies. The relative binding-free energy (ΔGbind) of each ligand molecule was calculated using MM-GBSA technique (Prime), and the findings are shown in Table 6. The ΔG_{bind} of selected compounds fell in the range of -33.4 to -48.4` kcal/mol indicating good binding affinity with TNF-α.

Table 6. Binding free energy calculation of selected 7 compounds using Prime/MM-GBSA approach.

S.No.	Name	ΔG_{bind}	ΔG_{bind} Coulomb	ΔG_{bind} Hbonnd	ΔG_{bind} Lipophilic	ΔG_{bind} Solv GB	ΔG_{bind} vdW
1	N6-(2-Phenylethyl)adenosine	-45.52	-12.45	-0.69	-24.83	22.23	-29.7
2	2-D08	-48.43	-26.04	-0.54	-20.03	20.23	-22.52
3	N-[(4-Aminophenyl)methyl]adenosine	-33.4	1.06	-0.62	-21.44	27.73	-39.72
4	5'-N-Ethylcarboxamidoadenosine	-46.23	5.89	-1.21	-19.99	7.99	-38.64
5	NM107	-47.79	-12.24	-1.61	-15.66	12.2	-30.1
6	Trifluridine	-42.11	-8.77	-0.49	-21.13	14.13	-27.55
7	APNEA	-43.61	-3.94	-0.91	-21.66	23.17	-35.34

Coulomb—Coulomb energy; **Hbond**—Hydrogen-bonding correction; **Lipo**—Lipophilic energy; **Solv GB**—Generalized Born electrostatic solvation energy; **vdW**—Van der Waals energy

Docking studies cannot reproduce the most realistic situation of ligand-protein interactions since any grid-based docking technique considers the receptor a rigid entity instead of solvating the system with water molecules. So, to further understand the stability of the best-identified hit and the non-bonding interaction between the ligand and protein, MD simulation was performed for 50 ns using the Desmond module of Schrödinger [54]. When exposed to these MD simulations, a system generates Newtonian dynamics, followed by a trajectory pathway for the axis coordinates, speed, and even the energies of the particles in the system [70].

Molecular Dynamic studies of N6-(2-Phenylethyl)adenosine, 2-D08, N-[(4Aminophenyl)methyl]adenosine, 5'-N-Ethylcarboxamidoadenosine, NM107, Trifluridine, and APNEA have provided comprehensive insights into the stability of protein–ligand interactions in a solvent system [71]. RMSD is a parameter that measures a relative change in atom displacement concerning a reference frame for a particular frame. When the system maintains low levels of RMSD with consistent fluctuations during the entire simulation, it is said to be equilibrated and stabilized; greater fluctuations, on the other hand, reflect low stability. RMSD fluctuations of about 1–3 Å are preferred for smaller proteins. In our findings, we observed acceptable variations in

protein RMSD values. The interaction of N6-(2-Phenylethyl)adenosine with TNF-α for a period of 50 ns showed that TNF-α was stable after 16 ns with the RMSD value between 2.1 Å to 2.5 Å whereas N6-(2-Phenylethyl)adenosine was seen to exhibit RMSD fluctuations between 7.1 Å and 11.8 Å after 5 ns, however the complex appeared to move apart, most likely owing to significant conformational changes in the protein as evident in Figure 8.

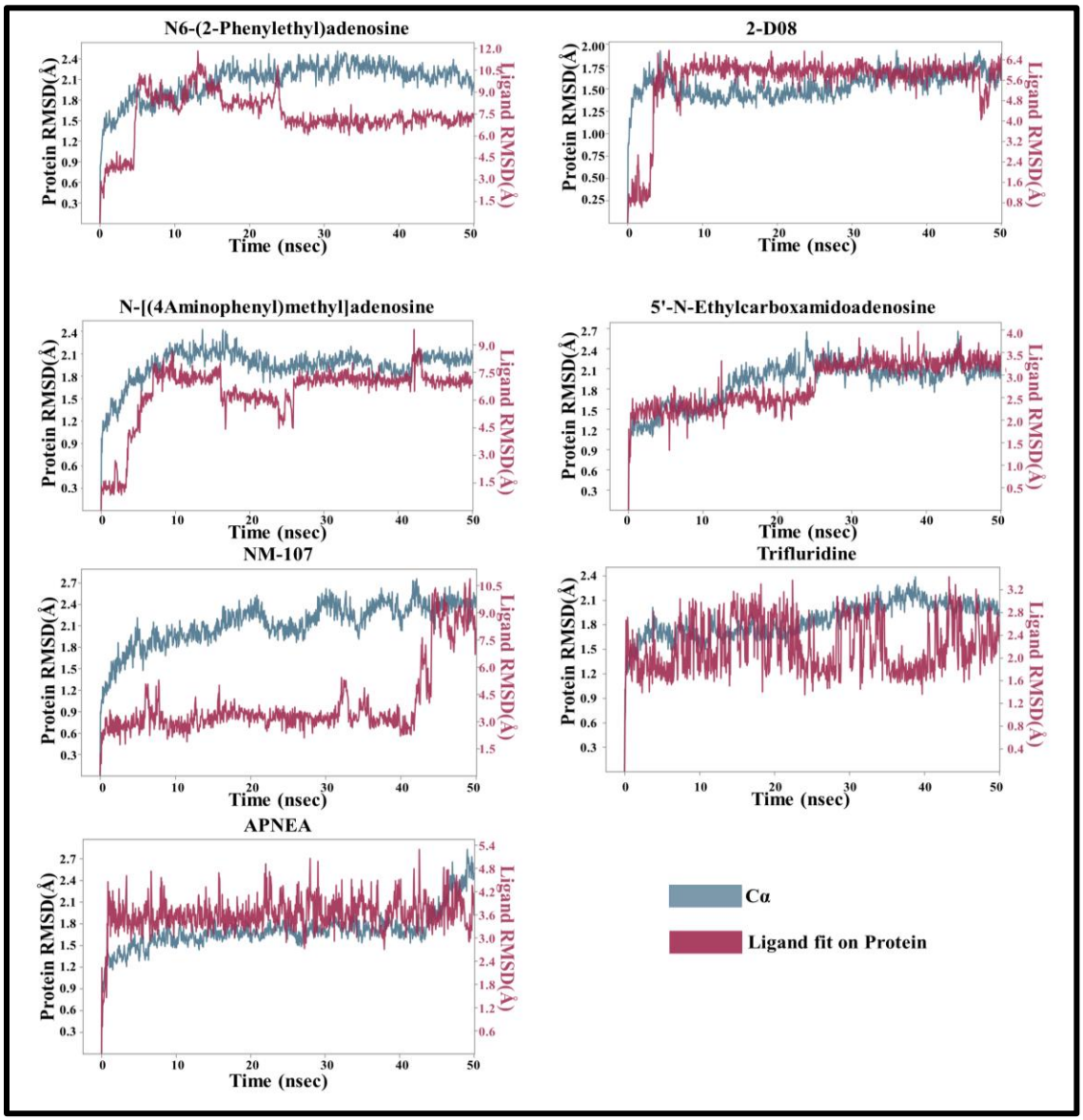

Figure 8. RMSD plots of ligands with TNF-α. The RMSD plots of N6-(2-Phenylethyl)adenosine, 2-D08, N-[(4Aminophenyl)methyl]adenosine, 5'-N-Ethylcarboxamidoadenosine, NM107, Trifluridine, and APNEA for simulations run for 50 ns.

The interaction of 2- DO8 with TNF-α throughout 50 ns revealed that the ligand and protein were stable with slight fluctuations within the specified limit and were close to each other after 5 ns; thus, the complex showed good stability. The interaction of N-[(4Aminophenyl)methyl]adenosine with TNF-α for a period of 50 ns showed that TNF-α was stable after 30 ns with the RMSD value between 1.8 Å to 2.1 Å whereas N-[(4Aminophenyl)methyl]adenosine was seen to exhibit RMSD fluctuations between 6.7 Å and 8.7

Å with proximity with each other, indicating a good contact between N-[(4Aminophenyl)methyl]adenosine and TNF-α as evident in Figure 8. The interaction of 5'-N-Ethylcarboxamidoadenosine with TNF-α for a period of 50 ns showed that TNF-α was stable after 25 ns with the RMSD value between 1.9 Å to 2.4 Å, whereas 5'-N-Ethylcarboxamidoadenosine was seen to exhibit RMSD fluctuations between 3.0 Å and 3.7 Å with proximity, indicating a good contact between N 5'-N-Ethylcarboxamidoadenosine and TNF-α. The NM107-TNF-α complex appeared to move apart, most likely owing to significant conformational changes in the protein. The interaction of Trifluridine with TNF-α for 50 ns revealed that the protein was stable throughout the run with an RMSD value between 1.3 Å and 2.4 Å, whereas Trifluridine was found to exhibit RMSD fluctuations between 1.4 Å and 3.4 Å with proximity with each other, indicating a good contact between Trifluridine and TNF-α. The interaction of APNEA with TNF-α for a period of 50 ns showed that TNF-α was stable after 6 ns with the RMSD value between 1.0 Å to 2.7 Å, whereas APNEA was seen to exhibit RMSD fluctuations between 3.0 Å and 4.6 Å with proximity, indicating a possibility of good contact.

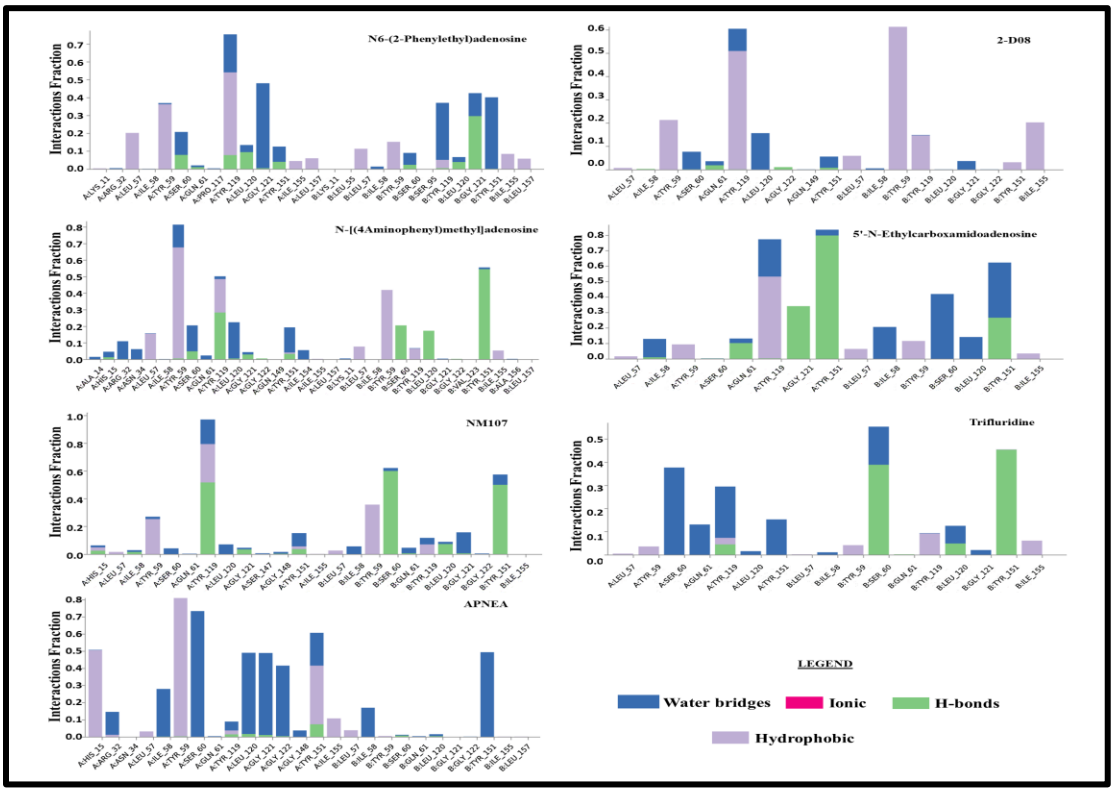

Figure 9. Protein Interaction with the ligands**.** The different contacts of N6-(2-Phenylethyl)adenosine, 2-D08, N-[(4Aminophenyl)methyl]adenosine, 5'-N-Ethylcarboxamidoadenosine, NM107, Trifluridine, and APNEA with various protein residues during the simulation of 50 ns.

Moreover, protein-ligand interactions must be tracked during the simulation. The hydrogen bonds are essential for ligand binding. Because of their considerable effect on drug selectivity, metabolization, and adsorption, hydrogen bonding characteristics must be considered during drug design. Hydrophobic contact is mediated by an aromatic or aliphatic group on the ligand and a hydrophobic amino acid. Interactions between two atoms with opposing charges within 3.7 Å of one another and do not include a hydrogen bond are known as ionic interactions. Water Bridges are protein-ligand interactions that include hydrogen bonds and are mediated by water molecules.

The protein-Ligand interaction diagram showed that N6-(2-Phenylethyl)adenosine, N-[(4Aminophenyl)methyl]adenosine, 5'-N-Ethylcarboxamidoadenosine, Trifluridine, and APNEA exhibited strong hydrogen bonding, hydrophobic interactions, and water bridges with TNF-α, but surprisingly the interaction of 2-D08 with TNF-α failed to show the desired contact with amino acids of TNF-α (Figure 9-10).

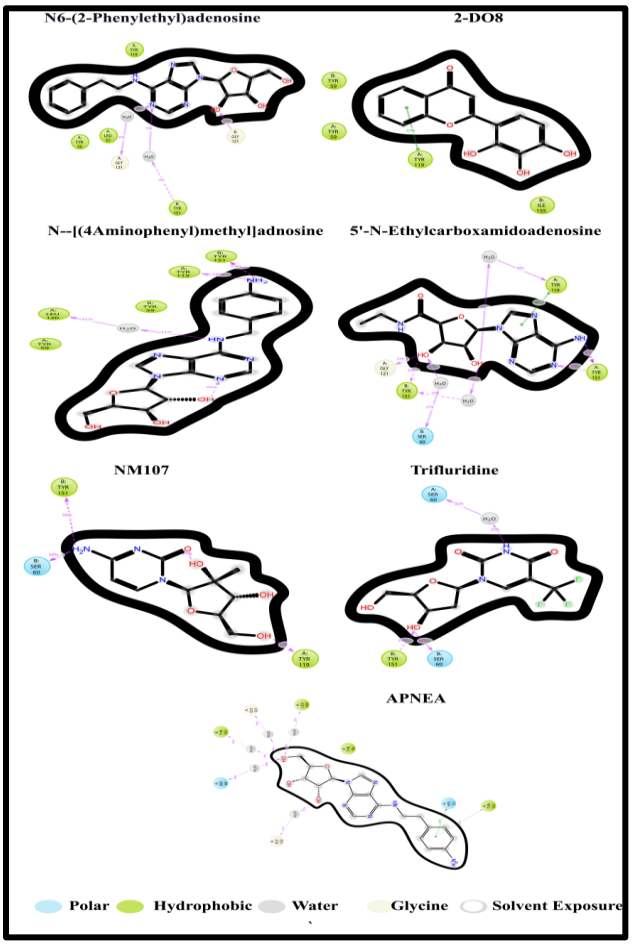

Figure 10. Protein-Ligand contacts**.** The 2D contacts of N6-(2-Phenylethyl)adenosine, 2-D08, N-[(4Aminophenyl)methyl]adenosine, 5'-N-Ethylcarboxamidoadenosine, NM107, Trifluridine, and APNEA with protein residues during the simulation of 50 ns.

Moreover, the ligand interaction diagram also revealed that LEU57, SER60 TYR59, GLN61, TYR119, GLY121, and TYR151 in chain A and LEU57, TYR59, SER60, TYR119, and TYR151 in chain B play an important role in ligand binding (Figure 9-10).

Protein Root Mean Square Fluctuation (P-RMSF) attributes were determined to better understand the behavior of individual amino acid residues throughout the simulation. Protein residues are essential for attaining a stable conformation in the protein-ligand complexes [72]. P-RMSF was monitored to assess the local changes along the protein chain. Our results showed that very few amino acids exhibited RMSF >3.0 Å during the simulations (Figure 11, Table 7). Moreover, low P-RMSF was observed during the respective protein-ligand interaction with the active binding site (green color), indicating the stability of protein when complexed with the respective compounds.

Table 7. Residue index of TNF–α complexed with selected 7 compounds showing P-RMSF >3.0 Å.

Ligand	Residue Index	Chain	RMSF Value (Å)
N6-(2-Phenylethyl)adenosine	22 (ALA)	A	3.19
2-D08	10 (ASP)	A	3.25
N-[(4Aminophenyl)methyl]adenosine	22 (ALA)	A	3.09
5'-N-Ethylcarboxamidoadenosine	87 (TYR)	B	3.11
NM107	86 (SER)	B	3.42
	87 (TYR)	B	3.41
Trifluridine	24 (GLY)	A	3.21
	108 (GLY)	A	3.13
APNEA	-	-	-

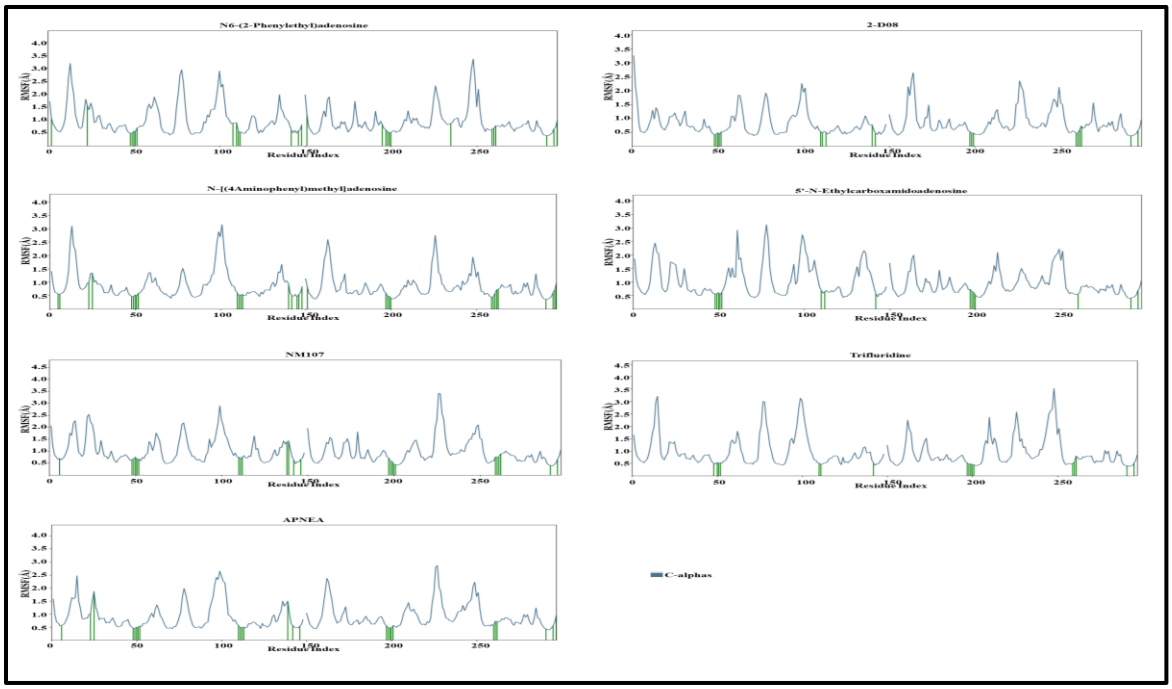

Figure 11. Protein Root Mean Square Fluctuation. The root mean square fluctuation plot for Cα of protein residues in complex with N6-(2-Phenylethyl)adenosine, 2-D08, N-[(4Aminophenyl)methyl]adenosine, 5'-N-Ethylcarboxamidoadenosine, NM107, Trifluridine, and APNEA, respectively during the simulation of 50 ns. The green color represents the binding site interacting with respective compounds; peaks indicate areas of the protein that fluctuate the most during the simulation.

The Ligand Root Mean Square Fluctuation (L-RMSF) characterizes variations in ligand atom positioning. The L-RMSF provides information on how ligand fragments interact with proteins and their entropic role in the binding events. Atoms of N6-(2-Phenylethyl)adenosine were highly fluctuated. Atoms of D08, ranging from 7 to 9, have RMSF > 2.5 Å, while other atoms possess low RMSF. Few atoms of 5'-N-Ethylcarboxamidoadenosine atoms exhibited moderate fluctuations **(**RMSF > 2. 0 Å.**)** Moreover, all atoms of Trifluridine and APNEA had very little fluctuations with RMSF < 1.7 Å. (Figure 12, Table 8).

Table 8. Highly fluctuated atoms of selected 7 compounds during MD simulation.

Ligand	Atom Index	RMSF Value (Å)	Ligand	Atom Index	RMSF Value (Å)
N6-(2-Phenylethyl)adenosine	23	5.05	5'-N-Ethylcarboxamidoadenosine	4	2.05
	24	5.62		5	2.29
	26	6.05		12	2.34
	26	5.94	NM107	2	4.01

	27	5.31		3	3.85
2-D08	7	2.86		7	4.58
	8	2.66	Trifluridine,	19	1.49
	9	3.11		9	1.45
N-[(4Aminophenyl)methyl]adenosine	1	3.70		10	1.45
	2	3.34	APNEA	28	1.61
	5	3.26		36	1.44
	7	3.30		25	1.38

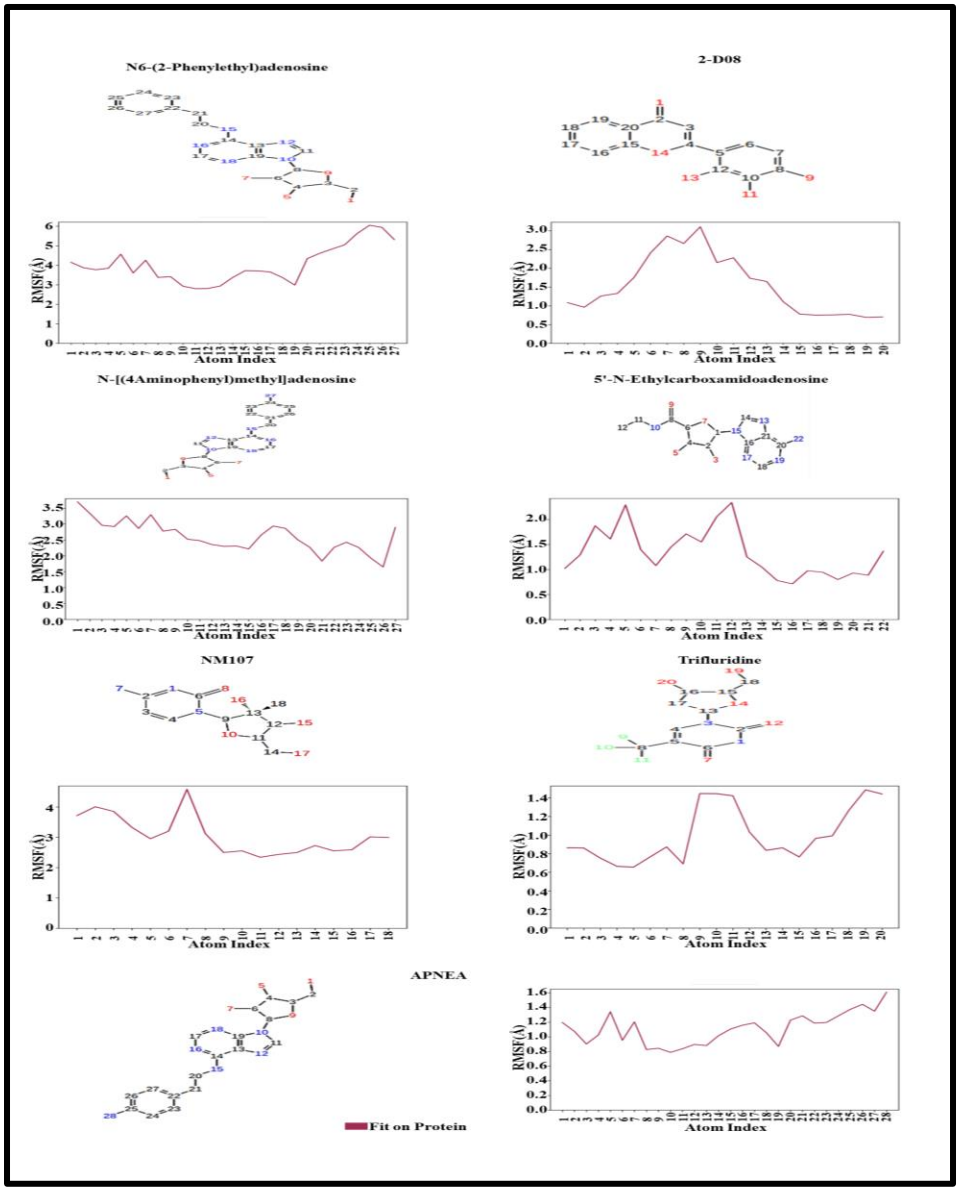

Figure 12. Ligand Root Mean Square Fluctuation. The root mean square fluctuation of the atoms in N6-(2-Phenylethyl)adenosine, 2-D08, N-[(4Aminophenyl)methyl]adenosine, 5'-N-Ethylcarboxamidoadenosine, NM107, Trifluridine, and APNEA as indicated in their numbering (top) during the simulation of 50 ns.

The protein RMSD, protein interaction diagram, P-RMSF, and L-RMSF demonstrated that the complex of TNF-α with N-[(4Aminophenyl)methyl]adenosine, 5'-N-Ethylcarboxamidoadenosine, Trifluridine, and APNEA was stable over 50 ns of the MD simulation with strong protein-ligand interactions.

4. Conclusions

TNF-α is directly implicated in the majority of inflammatory events in mammals. In this study, a total of 210 natural-like compounds were screened against TNF-α to determine their potential as TNF-α inhibitors. Based on the docking scores, 20 natural-like compounds showed promising binding affinities with docking score <-6.5, indicating good binding potential with TNF-α. However, by ADMET profiling, 7 compounds i.e. N6-(2-Phenylethyl)adenosine, 2-D08, N [(4Aminophenyl)methyl]adenosine, 5'-N-Ethylcarboxamidoadenosine, NM107, Trifluridine, and APNEA were identified as excellent drug-like molecules, which was further validated by MM-GBSA binding energies and MD simulation. The MM-GBSA and MD simulations finally revealed that 4 compounds, i.e., N-[(4Aminophenyl)methyl]adenosine, 5'-N Ethylcarboxamidoadenosine, Trifluridine, and APNEA have high binding affinities for TNF-α even in the presence of solvents, and counter ions thus may act as potential inhibitors of TNF-α. Nonetheless, additional *in vivo* and *in vitro* studies are required to validate these results.

Funding

ICMR Senior Research Fellowship supported this work to Vipul Agarwal (File No. 3/1/2(12)/CVD/2019-NCD-II).

Acknowledgments

The authors acknowledge ICMR and the Department of Pharmaceutical Sciences, Babasaheb Bhimrao Ambedkar University, for providing the necessary infrastructure.

Conflicts of Interest

The authors declare no conflict of interest. The funders had no role in the study's design, in the collection, analyses, or interpretation of data, in the writing of the manuscript, or in the decision to publish the results.

References

1. Sethi, J.K.; Hotamisligil, G.S. Metabolic Messengers: tumour necrosis factor. *Nat. Metab.* **2021**, *3*, 1302–1312, https://doi.org/10.1038/s42255-021-00470-z.
2. Parameswaran, N.; Patial, S. Tumor Necrosis Factor-α Signaling in Macrophages. *Crit. Rev. Eukaryot. Gene Expr.* **2010**, *20*, 87–103, https://doi.org/10.1615/critreveukargeneexpr.v20.i2.10.
3. Zaka, M.; Abbasi, B.H.; Durdagi, S. Novel tumor necrosis factor-α (TNF-α) inhibitors from small molecule library screening for their therapeutic activity profiles against rheumatoid arthritis using target-driven approaches and binary QSAR models. *J. Biomol. Struct. Dyn.* **2019**, *37*, 2464-2476, http://doi.org/10.1080/07391102.2018.1491423.
4. Giambelluca, M.; Rollet-Labelle, E.; Bertheau-Mailhot, G.; Laflamme, C.; Pouliot, M. Post-transcriptional regulation of tumour necrosis factor alpha biosynthesis: Relevance to the pathophysiology of rheumatoid arthritis. *OA Inflamm.* **2013**, *1*, 1–6.
5. Zia, K.; Ashraf, S.; Jabeen, A.; Saeed, M.; Nur-e-Alam, M.; Ahmed, S.; Al-Rehaily, A.J.; Ul-Haq, Z. Identification of potential TNF-α inhibitors: from in silico to in vitro studies. *Sci. Rep.* **2020**, *10*, 20974, http://doi.org/10.1038/s41598-020-77750-3.
6. Kim, O.T.P.; Le, M.D.; Trinh, H.X.; Nong, H.V. *In Silico* studies for the interaction of tumor necrosis factor-alpha (TNF-α) with different saponins from Vietnamese ginseng (*Panax vietnamesis*). *Biophys. Physicobiology* **2016**, *13*, 173–180, http://doi.org/10.2142/biophysico.13.0_173.
7. Matera, M.G.; Calzetta, L.; Cazzola, M. TNF-α inhibitors in asthma and COPD: We must not throw the baby out

with the bath water. *Pulm. Pharmacol. Ther.* **2010**, *23*, 121–128, http://doi.org/10.1016/j.pupt.2009.10.007.
8. Aldhalmi, A.K.; Al-Athari, A.J.H.; Makki Al-Hindy, H.A.-A. Association of Tumor Necrosis Factor-α and Myeloperoxidase Enzyme with Severe Asthma: A Comparative Study. *Reports Biochem. Mol. Biol.* **2022**, *11*, 238–245.
9. Niessen, N.M.; Gibson, P.G.; Baines, K.J.; Barker, D.; Yang, I.A.; Upham, J.W.; Reynolds, P.N.; Hodge, S.; James, A.L.; Jenkins, C.; Peters, M.J; Marks, G.B.; Baraket, M.; Simpson, J.L.; Fricker, M. Sputum TNF markers are increased in neutrophilic and severe asthma and are reduced by azithromycin treatment. *Allergy* **2021**, *76*, 2090–2101, https://doi.org/10.1111/all.14768.
10. Weyand, C.M.; Bryl, E.; Goronzy, J.J. The role of T cells in rheumatoid arthritis. *Arch. Immunol. Ther. Exp. (Warsz).* **2000**, *48*, 429–435.
11. Mease, P.J. Tumour necrosis factor (TNF) in psoriatic arthritis: pathophysiology and treatment with TNF inhibitors. *Ann. Rheum. Dis.* **2002**, *61*, 298–304, https://doi.org/10.1136/ard.61.4.298.
12. Liu, W.; Lu, X.; Shi, P.; Yang, G.; Zhou, Z.; Li, W.; Mao, X.; Jiang, D.; Chen, C. TNF-α increases breast cancer stem-like cells through up-regulating TAZ expression via the non-canonical NF-κB pathway. *Sci. Rep.* **2020**, *10*, 1804, https://doi.org/10.1038/s41598-020-58642-y.
13. Thomas, P.S. Tumour necrosis factor-α: The role of this multifunctional cytokine in asthma. *Immunol. Cell Biol.* **2001**, *79*, 132–140, http://doi.org/10.1046/j.1440-1711.2001.00980.x.
14. Agarwal, V.; Kaushik, A.S.; Rehman, M.; Chaudhary, R.; Jawaid, T.; Kamal, M.; Mishra, V. Interleukin-6 expression and its modulation by diacerein in a rat model of chronic stress induced cardiac dysfunction. *Heliyon* **2021**, *7*, e08522, http://doi.org/10.1016/j.heliyon.2021.e08522.
15. Peng, Z.; Peng, S.; Lin, K.; Zhao, B.; Wei, L.; Tuo, Q.; Liao, D.; Yuan, T.; Shi, Z. Chronic stress-induced depression requires the recruitment of peripheral Th17 cells into the brain. *J. Neuroinflammation* **2022**, *19*, 186, http://doi.org/10.1186/s12974-022-02543-6.
16. Petrinović, S.V.; Milošević, M.S.; Marković, D.; Momčilović, S. Interplay between stress and cancer-A focus on inflammation. *Front. Physiol.* **2023**, *14*, http://doi.org/10.3389/fphys.2023.1119095.
17. Sharma, A.; Singh, T.; Pathak, D.; Virmani, T.; Kumar, G.; Alhalmi, A. Antidepressive-Like Effect of *Aegle Marmelos* Leaf Extract in Chronic Unpredictable Mild Stress-Induced Depression-Like Behaviour in Rats. *Biomed Res. Int.* **2022**, *2022*, 6479953, http://doi.org/10.1155/2022/6479953.
18. Verma, H.; Shivavedi, N.; Tej, G.N.V.C.; Kumar, M.; Nayak, P.N. Prophylactic administration of rosmarinic acid ameliorates depression-associated cardiac abnormalities in Wistar rats: Evidence of serotonergic, oxidative, and inflammatory pathways. *J. Biochem. Mol. Toxicol.* **2022**, *36*, e23160, http://doi.org/10.1002/jbt.23160.
19. Gupta, G.L.; Sharma, L.; Sharma, M. 18β-Glycyrrhetinic Acid Ameliorates Neuroinflammation Linked Depressive Behavior Instigated by Chronic Unpredictable Mild Stress via Triggering BDNF/TrkB Signaling Pathway in Rats. *Neurochem. Res.* **2023**, *48*, 551–569, doi: http://doi.org/10.1007/s11064-022-03779-7.
20. Willrich, M.A.V.; Murray, D.L.; Snyder, M.R. Tumor necrosis factor inhibitors: clinical utility in autoimmune diseases. *Transl. Res.* **2015**, *165*, 270–282, http://doi.org/10.1016/j.trsl.2014.09.006.
21. Evangelatos, G.; Bamias, G.; Kitas, G.D.; Kollias, G.; Sfikakis, P.P. The second decade of anti-TNF-a therapy in clinical practice: new lessons and future directions in the COVID-19 era. *Rheumatol. Int.* **2022**, *42*, 1493–1511, http://doi.org/10.1007/s00296-022-05136 http://doi.org/-x.
22. Leone, G.M.; Mangano, K.; Petralia, M.C.; Nicoletti, F.; Fagone, P. Past, Present and (Foreseeable) Future of Biological Anti-TNF Alpha Therapy. *J. Clin. Med.* **2023**, *12*, 1630, http://doi.org/10.3390/jcm12041630.
23. Tracey, D.; Klareskog, L.; Sasso, E.H.; Salfeld, J.G.; Tak, P.P. Tumor necrosis factor antagonist mechanisms of action: A comprehensive review. *Pharmacol. Ther.* **2008**, *117*, 244–279, http://doi.org/10.1016/j.pharmthera.2007.10.001.
24. Dogra, S.; Khullar, G. Tumor necrosis factor-α antagonists: Side effects and their management. *Indian J. Dermatol. Venereol. Leprol.* **2013**, *79*, 35-46, http://doi.org/10.4103/0378-6323.115526.
25. Melagraki, G.; Ntougkos, E.; Papadopoulou, D.; Rinotas, V.; Leonis, G.; Douni, E.; Afantitis, A.; Kollias, G. *In Silico* Discovery of Plant-Origin Natural Product Inhibitors of Tumor Necrosis Factor (TNF) and Receptor Activator of NF-$_K$B Ligand (RANKL). *Front. Pharmacol.* **2018**, *9*, http://doi.org/10.3389/fphar.2018.00800.
26. Chan, D.S.H.; Lee, H.M.; Yang, F.; Che, C.M.; Wong, C.C.L.; Abagyan, R.; Leung, C.H.; Ma, D.L. Structure-Based Discovery of Natural-Product-like TNF-α Inhibitors. *Angew. Chemie. Int. Ed.* **2010**, *49*, 2860–2864, http://doi.org/10.1002/anie.200907360.
27. Leung, C.H.; Chan, D.S.H.; Kwan, M.H.T.; Cheng, Z.; Wong, C.Y.; Zhu, G.Y.; Fong, W.F.; Ma, D.L. Structure-Based Repurposing of FDA-Approved Drugs as TNF-α Inhibitors. *ChemMedChem.* **2011**, *6*, 765–768, http://doi.org/10.1002/cmdc.201100016.
28. Leung, C.H.; Zhong, H.J.; Yang, H.; Cheng, Z.; Chan, D.S.H.; Ma, V.P.Y.; Abagyan, R.; Wong, C.Y.; Ma, D.L. A Metal-Based Inhibitor of Tumor Necrosis Factor-α. *Angew. Chemie* **2012**, *124*, 9144–9148, http://doi.org/10.1002/ange.201202937 .
29. He, M.M.; Smith, A.S.; Oslob, J.D.; Flanagan, W.M.; Braisted, A.C.; Whitty, A.; Cancilla, M.T.; Wang, J.;

Lugovskoy, A.A.; Yoburn, J.C.; Fung, A.D.; Farrington, G.; Eldredge, J.K.; Day, E.S.; Cruz, L.A.; Cachero, T.G.; Miller, S.K.; Friedman, J.E.; Choong, I.C.; Cunningham, B.C. Small-Molecule Inhibition of TNF-Alpha. *Science* **2005**, *310*, 1022–1025, http://doi.org/10.1126/science.1116304 .
30. Shivaleela, B.; Srushti, S.C.; Shreedevi, S.J.; Babu, R.L. Thalidomide-based inhibitor for TNF-α: designing and *Insilico* evaluation. *Futur. J. Pharm. Sci.* **2022**, *8*, 5, http://doi.org/10.1186/s43094-021-00393-2.
31. Boyenle, I.D.; Adelusi, T.I.; Ogunlana, A.T.; Oluwabusola, R.A.; Ibrahim, N.O.; Tolulope, A.; Okikiola, O.S.; Adetunji, B.L.; Abioye, I.O.; Oyedele, A.Q.K. Consensus scoring-based virtual screening and molecular dynamics simulation of some TNF-alpha inhibitors. *Informatics Med. Unlocked* **2022**, *28*, 100833, http://doi.org/10.1016/j.imu.2021.100833.
32. Berman, H.M.; Westbrook, J.; Feng, Z.; Gilliland, G.; Bhat, T.N.; Weissig, H.; Shindyalov, I.N.; Bourne, P.E. The Protein Data Bank. *Nucleic Acids Res.* **2000**, *28*, 235–242, https://doi.org/10.1093/nar/28.1.235.
33. Schrödinger Release 2021-1: Epik 2021.
34. Sastry, G.M.; Adzhigirey, M.; Day, T.; Annabhimoju, R.; Sherman, W. Protein and ligand preparation: parameters, protocols, and influence on virtual screening enrichments. *J. Comput. Aided. Mol. Des.* **2013**, *27*, 221–234, https://doi.org/10.1007/s10822-013-9644-8.
35. Rajagopal, K.; Pandiselvi, A.; Gowramma, B.; Balachandran, P. In-Silico Design, ADMET Screening, MM-GBSA Binding Free Energy of Some Novel Isoxazole Substituted 9-Anilinoacridines as HER2 Inhibitors Targeting Breast Cancer. *Curr. Drug Res. Rev.* **2019**, *11*, 118-128, http://doi.org/10.2174/2589977511666190912154817.
36. Pirolli, D.; Righino, B.; Camponeschi, C.; Ria, F.; Di Sante, G.; De Rosa, M.C. Virtual screening and molecular dynamics simulations provide insight into repurposing drugs against SARS-CoV-2 variants spike protein/ACE2 interface. *Sci. Rep.* **2023**, *13*, 1494, http://doi.org/10.1038/s41598-023-28716-8.
37. Azam, M.A.; Jupudi, S. Extra precision docking, free energy calculation and molecular dynamics studies on glutamic acid derivatives as MurD inhibitors. *Comput. Biol. Chem.* **2017**, *69*, 55–63, https://doi.org/10.1016/j.compbiolchem.2017.05.004.
38. Schrödinger Release 2021-1: LigPrep, 2021.
39. Raj, V.; Lee, J.H.; Shim, J.J.; Lee, J. Antiviral activities of 4H-chromen-4-one scaffold-containing flavonoids against SARS-CoV-2 using computational and *in vitro* approaches. *J. Mol. Liq.* **2022**, *353*, 118775, https://doi.org/10.1016/j.molliq.2022.118775.
40. Raj, V.; Park, J.G.; Cho, K.H.; Choi, P.; Kim, T.; Ham, J.; Lee, J. Assessment of antiviral potencies of cannabinoids against SARS-CoV-2 using computational and in vitro approaches. *Int. J. Biol. Macromol.* **2021**, *168*, 474–485, https://doi.org/10.1016/j.ijbiomac.2020.12.020.
41. Michel, M.; Homan, E.J.; Wiita, E.; Pedersen, K.; Almlöf, I.; Gustavsson, A.L.; Lundbäck, T.; Helleday, T.; Berglund, U.W. *In Silico* Druggability Assessment of the NUDIX Hydrolase Protein Family as a Workflow for Target Prioritization. *Front. Chem.* **2020**, *8*, https://doi.org/10.3389/fchem.2020.00443.
42. Schrödinger Release 2021-1: Sitemap, 2021.
43. Schrödinger Release 2021-1: Glide, 2021.
44. Friesner, R.A.; Banks, J.L.; Murphy, R.B.; Halgren, T.A.; Klicic, J.J.; Mainz, D.T.; Repasky, M.P.; Knoll, E.H.; Shelley, M.; Perry, J.K.; Shaw, D.E.; Francis, P.; Shenkin, P.S. Glide: A New Approach for Rapid, Accurate Docking and Scoring. 1. Method and Assessment of Docking Accuracy. *J. Med. Chem.* **2004**, *47*, 1739–1749, https://doi.org/10.1021/jm0306430.
45. Bakchi, B.; Krishna, A.; Sreecharan, E.; Ganesh, V.B.J.; Niharika, M.; Maharshi, S.; Puttagunta, S.B.; Sigalapalli, D.K.; Bhandare, R.R.; Shaik, A.B. An overview on applications of SwissADME web tool in the design and development of anticancer, antitubercular and antimicrobial agents: A medicinal chemist's perspective. *J. Mol. Struct.* **2022**, *1259*, 132712, https://doi.org/10.1016/j.molstruc.2022.132712.
46. Knoll, K.E.; van der Walt, M.M.; Loots, D.T. *In Silico* Drug Discovery Strategies Identified ADMET Properties of Decoquinate RMB041 and Its Potential Drug Targets against *Mycobacterium Tuberculosis* . *Microbiol. Spectr.* **2022**, *10*, e0231521, https://doi.org/10.1128/spectrum.02315-21.
47. Daina, A.; Michielin, O.; Zoete, V. SwissADME: a free web tool to evaluate pharmacokinetics, drug-likeness and medicinal chemistry friendliness of small molecules. *Sci. Rep.* **2017**, *7*, 42717, https://doi.org/10.1038/srep42717.
48. Isyaku, Y.; Uzairu, A.; Uba, S. Computational studies of a series of 2-substituted phenyl-2-oxo-, 2-hydroxyl- and 2-acylloxyethylsulfonamides as potent anti-fungal agents. *Heliyon* **2020**, *6*, e03724, https://doi.org/10.1016/j.heliyon.2020.e03724.
49. Pires, D.E.V.; Blundell, T.L.; Ascher, D.B. pkCSM: Predicting Small-Molecule Pharmacokinetic and Toxicity Properties Using Graph-Based Signatures. *J. Med. Chem.* **2015**, *58*, 4066–4072, https://doi.org/10.1021/acs.jmedchem.5b00104.
50. Schrödinger Release 2021-1: Prime, 2021.
51. Harder, E.; Damm, W.; Maple, J.; Wu, C.; Reboul, M.; Xiang, J.Y.; Wang, L.; Lupyan, D.; Dahlgren, M.K.; Knight, J.L.; Kaus, J.W.; Cerutti, D.A.; Krilov, G.; Jorgensen, W.L.; Abel, R.; Friesner, R.A. OPLS3: A Force

Field Providing Broad Coverage of Drug-like Small Molecules and Proteins. *J. Chem. Theory Comput.* **2016**, *12*, 281-296, https://doi.org/10.1021/acs.jctc.5b00864.
52. Balaji, B.; Ramanathan, M. Prediction of estrogen receptor β ligands potency and selectivity by docking and MM-GBSA scoring methods using three different scaffolds. *J. Enzyme Inhib. Med. Chem.* **2012**, *27*, 832–844, https://doi.org/10.3109/14756366.2011.618990.
53. Halder, D.; Das, S.; Joseph, A.; Jeyaprakash, R.S. Molecular docking and dynamics approach to in silico drug repurposing for inflammatory bowels disease by targeting TNF alpha. *J. Biomol. Struct. Dyn.* **2023**, *41*, 3462-3475, https://doi.org/10.1080/07391102.2022.2050948.
54. Kumar, A.; Rathi, E.; Kini, S.G. E-pharmacophore modelling, virtual screening, molecular dynamics simulations and in-silico ADME analysis for identification of potential E6 inhibitors against cervical cancer. *J. Mol. Struct.* **2019**, *1189*, 299–306, https://doi.org/10.1016/j.molstruc.2019.04.023.
55. Schrödinger Release 2021-1: Desmond Molecular Dynamics System, 2021.
56. John, A.; Umashankar, V.; Krishnakumar, S.; Deepa, P.R. Comparative Modeling and Molecular Dynamics Simulation of Substrate Binding in Human Fatty Acid Synthase: Enoyl Reductase and β-Ketoacyl Reductase Catalytic Domains. *Genomics Inform.* **2015**, *13*, 15–24, https://doi.org/10.5808/GI.2015.13.1.15.
57. Alama, M.S.; Otsukaa,S.; Wongb, N.; Abbasia, A.; Gaidad, M.M.; Fan, Y.; Daoud, M.; Ashwell, J..A. TNF plays a crucial role in inflammation by signaling via T cell TNFR2. *Proc. Natl. Acad. Sci. U.S.A.* **2021**, *118*, e2109972118, https://doi.org/10.1073/pnas.210997211.
58. Oladejo, D.O.; Duselu, G.O.; Dokunmu, T.M.; Isewon, I.; Oyelade, J.; Okafor, E.; Iweala, E.E.; Adebiyi, E. *In Silico* Structure Prediction, Molecular Docking, and Dynamic Simulation of *Plasmodium falciparum* AP2-I Transcription Factor. *Bioinform. Biol. Insights* **2023**, *17*,https://doi.org/10.1177/11779322221149616.
59. Saddala, M.S.; Huang, H. Identification of novel inhibitors for TNFα, TNFR1 and TNFα-TNFR1 complex using pharmacophore-based approaches. *J. Transl. Med.* **2019**, *17*, 215, https://doi.org/10.1186/s12967-019-1965-5.
60. Raj, V.; Aboumanei, M.H.; Rai, A.; Verma, S.P.; Singh, A.K.; Keshari, A.K.; Saha, S. Pharmacophore and 3d-Qsar Modeling of new 1,3,4-Thiadiazole Derivatives: Specificity to Colorectal Cancer. *Pharm. Chem. J.* **2020**, *54*, 12–25, https://doi.org/10.1007/s11094-020-02149-3.
61. Krüger, A.; Maltarollo, V.G.; Wrenger, C.; Kronenberger, T. ADME Profiling in Drug Discovery and a New Path Paved on Silica. In Book Drug Discovery and Development - New Advances 2019, Edited by Vishwanath Gaitonde, Partha Karmakar and Ashit Trivedi, http://doi.org/10.5772/intechopen.86174
62. Wu, F.; Zhou, Y.; Li, L.; Shen, X.; Chen, G.; Wang, X.; Liang, X.; Tan, M.; Huang, Z. Computational Approaches in Preclinical Studies on Drug Discovery and Development. *Front. Chem.* **2020**, *8*, 726, https://doi.org/10.3389/fchem.2020.00726.
63. Rettie, A.E.; Jones, J.P. CLINICAL AND TOXICOLOGICAL RELEVANCE OF CYP2C9: Drug-Drug Interactions and Pharmacogenetics. *Annu. Rev. Pharmacol. Toxicol.* **2005**, *45*, 477–494, https://doi.org/10.1146/annurev.pharmtox.45.120403.095821.
64. Wang, K.; Gao, Q.; Zhang, T.; Rao, J.; Ding, L.; Qiu, F. Inhibition of CYP2C9 by natural products: insight into the potential risk of herb-drug interactions. *Drug Metab. Rev.* **2020**, *52*, 235–257, https://doi.org/10.1080/03602532.2020.1758714.
65. Daly, A.K.; Rettie, A.E.; Fowler, D.M.; Miners, J.O. Pharmacogenomics of CYP2C9: Functional and Clinical Considerations. *J. Pers. Med.* **2017**, *8*, 1, https://doi.org/10.3390/jpm8010001.
66. Stergiopoulos, C.; Tsopelas, F.; Valko, K. Prediction of hERG inhibition of drug discovery compounds using biomimetic HPLC measurements. *ADMET DMPK* **2021**, *9*, 191–207, https://doi.org/10.5599/admet.995.
67. Krishna, S.; Borrel, A.; Huang, R.; Zhao, J.; Xia, M.; Kleinstreuer, N. High-Throughput Chemical Screening and Structure-Based Models to Predict hERG Inhibition. *Biology* **2022**, *11*, 209, https://doi.org/10.3390/biology11020209.
68. Borra, S.S.; Jane, N.R.; Palaniappan, D.; Subramanian, R.; Patankar, M.A.; Krishnamoorthy, S.G.; Parthasarathy, A.K. Genetic polymorphism of organic cation transporter 2 (OCT_2) and its effects on the pharmacokinetics and pharmacodynamics of Metformin: a narrative review *Egypt. J. Med. Hum. Genet.* **2023**, *24*, 13, https://doi.org/10.1186/s43042-023-00388-z.
69. Genheden, S.; Ryde, U. The MM/PBSA and MM/GBSA methods to estimate ligand-binding affinities. *Expert Opin. Drug Discov.* **2015**, *10*, 449-461, https://doi.org/10.1517/17460441.2015.1032936.
70. Choudhary, M.I.; Shaikh, M.; tul-Wahab, A.; ur-Rahman, A. *In silico* identification of potential inhibitors of key SARS-CoV-2 3CL hydrolase (Mpro) *via* molecular docking, MMGBSA predictive binding energy calculations, and molecular dynamics simulation. *PLoS One* **2020**, *15*, e0235030, https://doi.org/10.1371/journal.pone.0235030.
71. Chauhan, D.; Kumar, S.; Hashim, S.R.; Raj, V. Pharmacophore Generation, Quantitative Structure-Activity Relationship (QSAR), and Molecular Dynamic Simulation of Newly Substituted N-(6- Chloro-3-cyano-4-phenyl-4H-chromen-2-yl)-2-(4-chloro-phenoxy)-acetamide for Anticancer Activity. *Curr. Comput. Aided. Drug Des.* **2021**, *17*, 504–510, https://doi.org/10.2174/1573409916666200525150410.

72. Owoloye, A.J.; Ligali, F.C.; Enejoh, O.A.; Musa, A.Z.; Aina, O.; Idowu, E.T.; Oyebola, K.M. Molecular docking, simulation and binding free energy analysis of small molecules as P*f*HT1 inhibitors. *PLoS One* **2022**, *17*, e0268269, https://doi.org/10.1371/journal.pone.0268269.